An acoustic impedance investigation of spray-on foam insulation to detect bonding condition

by

Matthew Murray McKee

A thesis submitted to the graduate faculty

in partial fulfillment of the requirements for the degree of

MASTER OF SCIENCE

Major: Engineering Mechanics

Program of Study Committee:
J. A. Mann, Major Professor
Atul Kelkar
David Hsu
Judy Vance

Iowa State University

Ames, Iowa

2004

Graduate College
Iowa State University

This is to certify that the master's thesis of

Matthew Murray McKee

has met the thesis requirements of Iowa State University

Signatures have been redacted for privacy

TABLE OF CONTENTS

CHAPTER 1. INTRODUCTION

This thesis describes an investigation into the feasibility of using acoustic impedance as a measure to detect un-bonded areas of Spray-On Foam Insulation (SOFI). The SOFI is the material used to keep the external fuel tank on the space shuttle launch vehicle from icing due to the low temperature liquid fuel in the tank.

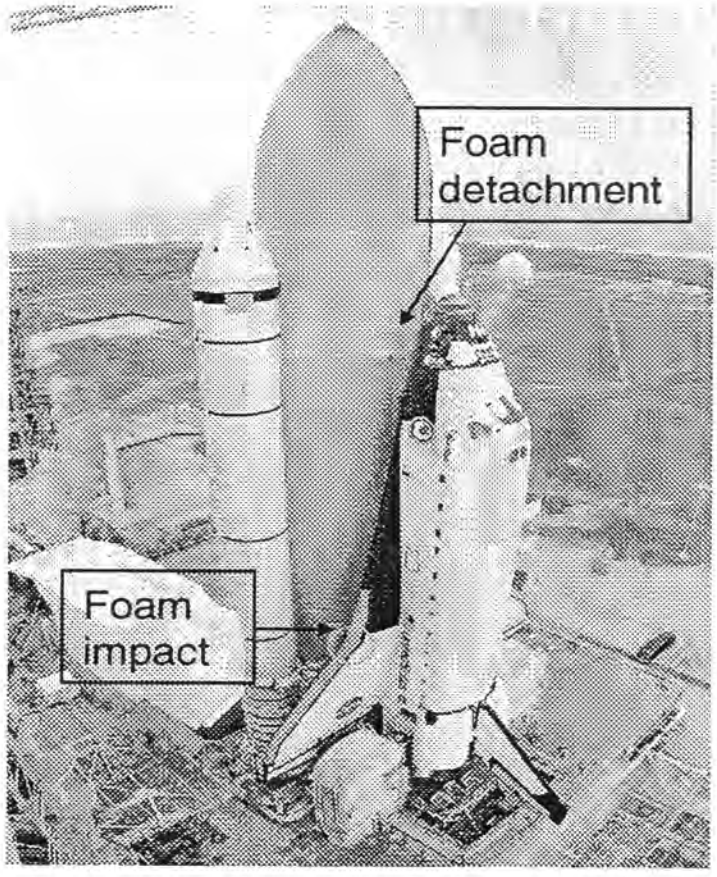

Figure 1.1 The shuttle Columbia on the launch pad prior to lift-off on its final mission.

1.1 Background on the Spray-On Foam Insulation Problem

On February 1st 2003 the space shuttle Columbia was lost during atmospheric reentry. The cause for this accident was found to be a section of insulating SOFI impacting the leading edge of the orbiters wing. The SOFI had broken off of the large liquid propellant tank in the area around the bipod that connects the orbiter to the tank. After breaking off, this large section of SOFI impacted on the left wing of the shuttle craft, causing significant damage to the Reinforced Carbon-Carbon (RCC) tiles on the leading edge of the wing. With the RCC tiles on the wing leading edge compromised, the shuttle craft disintegrated on reentry, spreading debris over several thousand square miles of Texas and surrounding states.

The RCC tiles are fragile enough that even pressing a thumbnail against them will leave a mark. They are only rated for impacts with kinetic energy less than 0.006 foot-pounds. This leaves the orbiter vulnerable to bird strikes, launch debris, ice and even SOFI impact. Analysis of the launch tracking photography lead the National Aeronautics and Space Administration (NASA) to believe that the SOFI piece that broke off of the Columbia had a speed relative to the orbiters wing of 582 miles per hour when it impacted the orbiters wing, and while the SOFI itself has a density of only 0.04 grams per cubic centimeter, the high velocity of the SOFI puts its energy well above the 0.006 foot-pound limit.

The SOFI is used to keep the liquid fuel tanks free of ice while on the ground, this was done because the impact of ice on the orbiter skin was such a concern. Because the RCC tiles are so fragile, the external fuel tanks must be well insulated to prevent ice build up while the orbiter sits on the launch pad. The SOFI does this job well, while the inside of the liquid fuel tanks is below -200 degrees Fahrenheit, the surface of the SOFI, barely 2 inches away is only slightly cool to the touch. The SOFI is machine-sprayed onto the external fuel tank approximately 1 to 2 inches thick across the surface, with thicker sections hand-sculpted around difficult geometries like the bipod.

The problem of SOFI breaking off the external fuel tank and impacting the orbiter was a problem that had existed since the first shuttle launches. Video of the launches taken from the launch tower shows a shower of particles from the launch vehicle as the shuttle lifts off. These particles are ice and SOFI from the external fuel tank and hoses containing liquid

fuel. Initially, this particle shower caused great concern to the NASA engineers, but as launches continued and no serious problems developed, the concern faded. With continued successful landings, SOFI strikes on the RCC tiles stopped being a "safety of flight" issue and became a simple, expected maintenance and turnaround time issue. It is important to note that the orbiter typically has 10-30 RCC tiles that need replaced after each mission.

That the bipod section of SOFI could break off was also a known phenomenon. It was known to have occurred six times before the Columbia's final flight. Four of those six occurrences were on Columbia flights. NASA may have been faulted for not examining this data closely as a possible problem with Columbia, but the Columbia Accident Investigation Board (CAIB) decided that this was not statistically significant because prior to the mid-90's the only orbiters with cameras installed in the belly that could image the external fuel tank as it fell away from the orbiter were the Challenger and the Columbia. This created a bias in the data toward the Columbia as many more images were available to analyze. In the mid-90's, all the remaining orbiters were fitted with belly cameras to record this and other events.

Perhaps most ominous is what happened to the orbiter Atlantis on flight STS-27R. Analysis of launch tracking imagery showed a debris impact about a minute and a half into the flight. The crew was asked by Mission Control to use the orbiters robotic arm, which is equipped with a camera, to image the orbiters belly. The Mission Commander, R. L. Gibson stated that the Atlantis "looked like it had been blasted by a shotgun." When the Atlantis landed NASA was shocked at the extent of the damage. There were 707 dings in the RCC tiles, 298 of which were greater than 1 inch in diameter. Even more worrying was that one entire tile had been knocked away, exposing the skin of the orbiter to the heat of reentry. The tile that was lost occurred over a thick aluminum plate which protected sensitive equipment. If the aluminum plate had not been as thick as the location of the lost tile, a burn through might have occurred for the Atlantis.

The cause of SOFI loss is currently unknown, but may be attributed to one or more of the following factors. The SOFI may not be properly bonded to the aluminum tank when it is applied. The SOFI may have air gaps in the interior of the SOFI, these air gaps may magnify the aerodynamic loads, or if they are close enough to the liquid fuel, the temperature inside the air gaps may be low enough that any air contained within them will liquefy, when this

liquid air goes through the quick temperature change at launch, NASA is concerned that the liquid air will become a gas quickly and simply blow a section of SOFI off the external tank.

To analyze the bonding, a method must be developed to detect the bonding condition of the SOFI to the aluminum tank. Several different methods are under development for this application. Terahertz radiation is being used at Rensselaer Polytechnic Institute to attempt to detect the bonding condition [Narayanan]. Terahertz radiation is in the far-infrared region of the electromagnetic spectrum, between microwaves and visible light. The SOFI is well suited to these measurements as it has a low attenuation of the terahertz radiation, allowing the radiation to penetrate to a depth of several inches into the SOFI.

Ultrasonic measurements were tested by Dr. D. K. Hsu at the Center for Non-Destructive Evaluation (CNDE) at Iowa State University (ISU). This method worked well in a measurement with the source on one side and the receiver on the other side, but the inside of the tank is inaccessible to place ultrasonic transducers when the SOFI is applied to the external fuel tank. Dr. Hsu attempted a one-sided measurement using ultrasonic methods but the layered nature of the SOFI made it impossible to detect the condition of the SOFI-aluminum interface with these methods. While ultrasonics is a well tested method, the ultrasonic energy can not effectively penetrate to the SOFI/aluminum bond.

As the terahertz and ultrasonic testing methods, NASA needs a method to identify areas where the SOFI is not bonded to the base aluminum. The key issue is that the detection of un-bonded areas must be done from the surface of the SOFI, not from the aluminum surface. This thesis will study the use of lower frequency sound, below 10,000 Hz, since the lower frequency sound can more readily penetrate the SOFI because of the longer wavelengths compared to the ultrasonic methods. Further acoustic impedance will be investigated as a means to quantify how the SOFI is interacting with the incident audible sound, based on a hypothesis that the bonding will influence how the SOFI reacts to the incident sound.

1.2 Problem Statement

Measurements of the acoustic impedance of the surface of a SOFI sample will be investigated as a means to identify de-bonding between the SOFI and the base metal. Further, the sensitivity of the impedance measurement to the acoustic environment, such as reflections and background noise will be evaluated.

1.3 Thesis Outline

The background, theory and rationale for investigating acoustic impedance is presented in Chapter 2. The issues involved in performing the impedance measurement and the test setup will be described in Chapter 3. The results are presented in Chapter 4 followed by a summary, a list of conclusions, and recommendations for future work in Chapter 5.

CHAPTER 2. THEORY

Two key assumptions in the behavior of the SOFI are being used for the research. The first is that the acoustic properties of the SOFI surface, as quantified by the surface acoustic impedance, is sensitive to the bonding between the SOFI and the backing metal. Second, the impedance at a point on the surface is dominated by the behavior of the SOFI in a small area around that point, rather than the whole SOFI sample. This second assumption allows the method to have a finite spatial resolution.

The definition of impedance, the theories behind the two assumptions and the method used to measure impedance are described.

2.1 Impedance

The acoustic impedance is a complex quantity defined by

$$Z = \frac{P}{\vec{u} \bullet \hat{n}}, \qquad [2.1]$$

where Z is the impedance P is the pressure, $\vec{u}$ is the particle velocity and $\hat{n}$ is a unit vector in a specified direction. When defining the acoustic impedance of a material, $\hat{n}$ is normal to the material surface. Impedance is used to quantify many boundary conditions in acoustics, such as source radiation, cavity resonance and the response of structures and materials to incident sound. It is this latter application of impedance that will be used in this thesis to identify defects in the SOFI bonding.

Impedance is a complex quantity. The real part of impedance is related to sound power. Therefore the sound power absorbed by a material can be directly related to the real part of impedance.

A classic technique in architectural acoustics to enhance the absorption of an absorption material, is to stand the material away from the rigid boundary with an air gap [Lord, et. al.], Figure 2.1. If a typical acoustic absorber is placed with a fixed-free boundary condition, Figure 2.1a, it will have a given impedance. If that same absorber, with the same thickness, is then placed with a free-free boundary condition and an air gap between it and the fixed surface, the impedance will change greatly at a frequency corresponding to the resonance of the air gap, Figure 2.1b. The depth of the air gap is chosen to maximize the energy absorbed by the material in a chosen frequency band. Changing the gap changes the frequency of peak absorption. It is assumed that the mechanism for changing the impedance of the surface of the material is a change in the impedance at the opposite boundary of the material. Therefore, in using impedance to examine the SOFI-aluminum bonding condition the assumption is made that the bonding condition will change the impedance at the SOFI-aluminum interface.

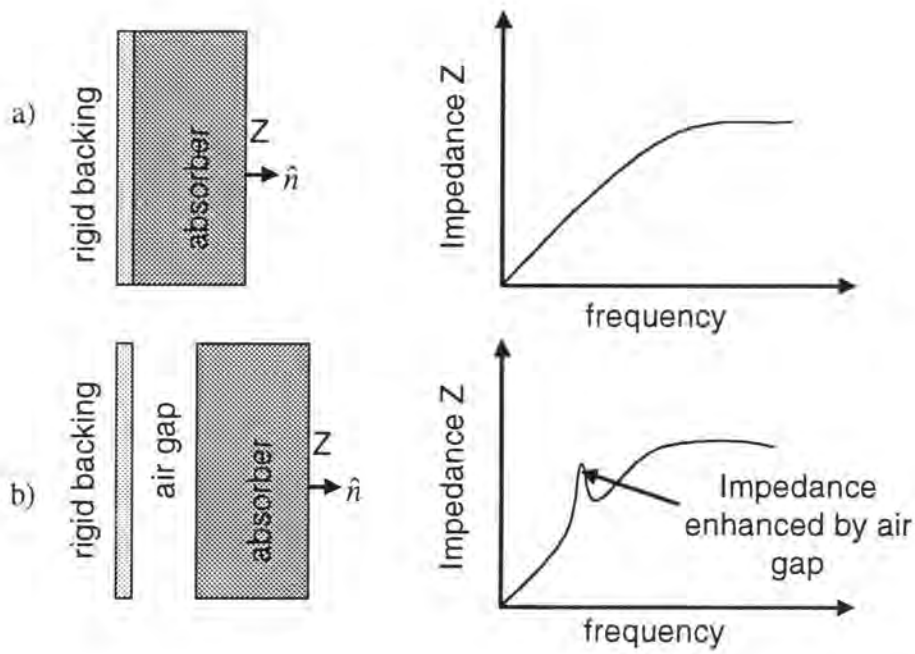

Figure 2.1 Idealization of the impedance of a a) fixed-free absorber and b) the impedance of a free-free absorber

Based on the above analysis, it can be expected that the real part of impedance, which is related to power, will increase above an un-bonded area, because the un-bonded location will absorb more sound due to the dis-bond. Following this logic, the thesis research was initiated, assuming that the condition of the bonding between the SOFI and the metal plate will change the absorption characteristics of the SOFI. Further, it was hypothesized that the acoustic impedance could detect the absorption change.

2.2 Locally Reacting

An important assumption in this thesis was that the SOFI was locally reacting. When a material is locally reacting then the material reacts to incident sound based on the properties of the material and the incident sound in a region surrounding the incident point, and does not depend on the bulk behavior of the structure. For example, a sound incident on a thin plate would not be a locally reacting condition because the plate as a whole will vibrate in patterns related to the vibration modes of a plate. By assuming that the SOFI is locally reacting, then the response of the SOFI can be modeled as shown in Figure 2.2. Instead of

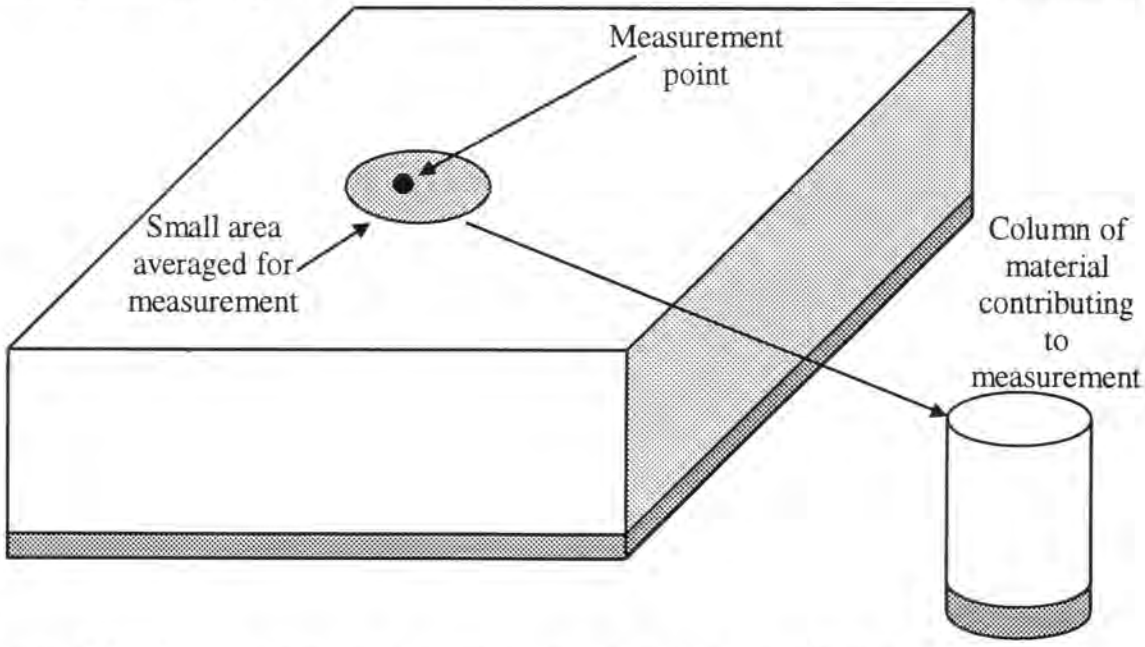

Figure 2.2 Schematic showing the modeling of a section of the SOFI and metal backing, if the locally reacting assumption holds.

modeling the material as a whole structure, a small cross section of the material can be modeled. Therefore only phenomena in the small cross section are needed to predict how the SOFI reacts to sound at each point along the SOFI surface. Typically these points can be separated by distances that are less than an acoustic wavelength. This assumption leads to a measurement that is sensitive to the SOFI material at each measurement point.

2.3 Finite Duct Theory

Using the assumption of a locally reacting material, a small area of SOFI, Figure 2.2, can be modeled alone. With normal incident sound, the size of the area is small enough to assume plane wave propagation in the material. A finite duct has similar behavior. The finite duct model is used because it has been widely analyzed for low frequencies, where there are guaranteed plane waves in the duct. The plane wave assumption matches those already used for the measurement method and the experiment setup that will be used. Therefore, one dimensional theory for a finite duct will be used to show that the impedance of the surface of the SOFI will depend on the impedance at the SOFI-aluminum interface.

Assuming that the sound incident on the SOFI surface will produce plane waves in the small SOFI area, the model shown in Figure 2.3 will be used. With this model, the sound is incident on the SOFI outer surface with impedance Z_0, the SOFI will have a depth L, the

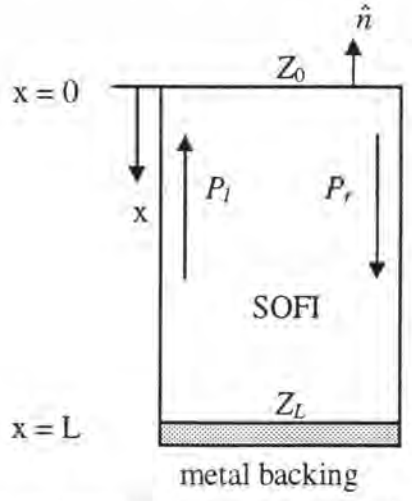

Figure 2.3 The finite duct approach to the impedance of the SOFI.

impedance at the SOFI-metal backing interface is Z_L, the speed of sound in the SOFI is c and the SOFI density is ρ. Within the SOFI, there are plane waves propagating in the two directions, P_l and P_r, representing the sum of all waves propagating in each direction. The finite duct conditions and assumptions can be applied to the column of SOFI in Figure 2.3 because we have assumed plane waves in the SOFI and made the assumption of a locally reacting surface. It can be shown, through the derived equations that Z_0 depends on Z_L.

Since P_r and P_l are the plane waves, they have the forms,

$$P_r = Ae^{j(\omega t - kx)} \qquad [2.5]$$

and

$$P_l = Be^{j(\omega t + kx)}, \qquad [2.6]$$

where t is time, x is position through the SOFI thickness, with the SOFI-air interface at x = 0 and the bond between the SOFI and the metal backing at x = L,

$$\omega = 2\pi f \qquad [2.7]$$

and

$$k = \frac{\omega}{c}. \qquad [2.8]$$

To calculate impedance velocity is also required, which for a plane wave has the form

$$u_r = \frac{A}{\rho c} e^{j(\omega t - kx)} \qquad [2.7]$$

and

$$u_l = \frac{B}{\rho c} e^{j(\omega t + kx)}. \qquad [2.8]$$

Using superposition, the impedance normal to the SOFI surface is

$$Z = \frac{P}{u} = \frac{Ae^{-jkx} + Be^{jkx}}{Ae^{-jkx} - Be^{jkx}} \rho c. \qquad [2.9]$$

At the SOFI surface, the impedance Z_0 is equated to Equation 2.9 with x = 0,

$$Z_0 = \frac{A+B}{A-B} \rho c, \qquad [2.10]$$

while the impedance Z_L is equated to Equation 2.9 with x = L,

$$Z_L = \frac{Ae^{-jkL} + Be^{jkL}}{Ae^{-jkL} - Be^{jkL}} \rho c . \qquad [2.11]$$

If the equations for Z_L and Z_0 are separately solved for the ratio A/B then

$$\frac{A}{B} = \frac{Z_0 + \rho c}{Z_0 - \rho c} = \frac{Z_L e^{jkL} + \rho c e^{jkL}}{Z_L e^{-jkL} + \rho c e^{-jkL}} . \qquad [2.12]$$

It is then possible to solve for Z_0

$$Z_0 = \left(\frac{\frac{Z_L}{\rho c} + j \tan(kL)}{1 + j \frac{Z_L}{\rho c} \tan(kL)} \right) \rho c . \qquad [2.13]$$

Therefore, Z_0, the impedance at the surface, depends on Z_L, the impedance at the SOFI-aluminum interface. Assuming that Z_L is dependent on the bonding condition, then Z_0, which is dependent on Z_L, will also be dependent on the bonding condition. This shows that a measurement of the surface impedance of the SOFI will be sensitive to the bonding condition at the SOFI-aluminum interface.

Analysis of Equation 2.13 is typically used to calculate the resonance frequencies of a finite length duct, defined as frequencies where the input impedance, Z_0, is zero. In the case of the SOFI the resonances will be thickness resonances. These frequencies will not only depend on the speed of sound but also on the impedance at the SOFI-aluminum interface. Therefore, it is expected that the resonance frequencies of the sound in the SOFI, as measured by the surface impedance, are dependent on the bond between the SOFI and the backing metal.

For the SOFI studied, the speed of sound in the SOFI was reported as approximately 500 m/s, D. K. Hsu, private communication. Since the SOFI is 2 inches thick, the quarter wavelength resonance is around 2500 Hz, and the half wavelength resonance is around 5000 Hz. These frequency ranges will be explored in the experimental studies.

2.4 Two Microphone Method

A number of different methods to measure impedance were evaluated [Dickinson and Doak], [Allard et. al.], [Allard and Aknine], [Seybert and Ross], [Cramond and Don], [Carles

et. al.], [Lahti], and [Legouis and Nicolas]. The one that was chosen was a simple method involving 2 microphones [Allard and Seiben]. Previous to the Allard and Seiben paper, impedance measurements required a sample of material that was 10 square meters or greater. The two microphone method was developed to allow acoustic impedance measurements to be done on smaller samples. This is ideal for this thesis research because the sample of SOFI that was supplied by NASA was small, about 0.31 square meters. This is another reason to support the assumption of locally reacting.

Impedance cannot be measured directly, because it is not possible to simultaneously measure velocity and pressure, and velocity is not measured directly. However, velocity can be estimated with a finite difference approximation [Fahy]. Consider measuring the pressure at two points using two microphones, Figure 2.4. If p_1 and p_2 are the pressures at the two microphones then the pressure at the mid-point between the two microphones will be approximated by

$$P(\omega) = \frac{p_1(\omega) + p_2(\omega)}{2}, \qquad [2.14]$$

and the velocity at the mid-point is

$$u(\omega) = \frac{-1}{j\omega\rho}\frac{\partial p(\omega)}{\partial x} \qquad [2.15]$$

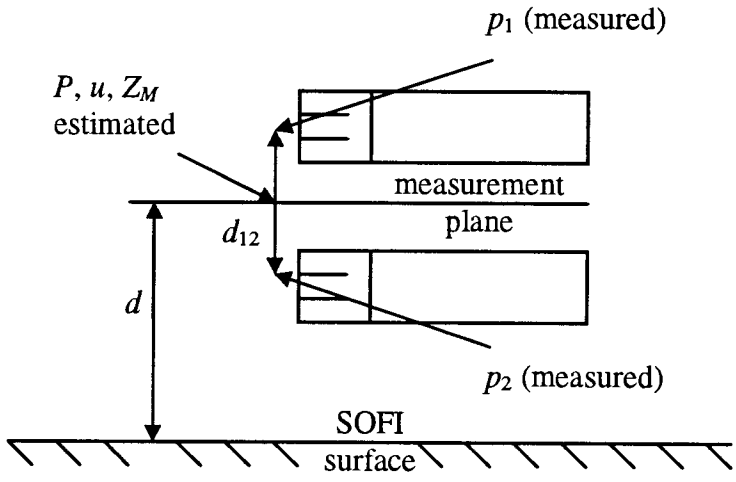

Figure 2.4 Two microphones used for estimating impedance

by approximating the spatial derivative of the pressure with a finite difference, the velocity is

$$u(\omega)=\frac{-1}{j\omega\rho}\left(\frac{p_2(\omega)-p_1(\omega)}{d_{12}}\right), \qquad [2.16]$$

where d_{12} is the distance between the microphones. Using Equations 2.14 and 2.16 and the definition of impedance, Equation 2.1, the estimate of impedance is

$$Z_M(\omega)=\frac{i\omega\rho d_{12}}{2}\frac{(p_1(\omega)+p_2(\omega))}{(p_2(\omega)-p_1(\omega))}. \qquad [2.17]$$

By defining the ratio of p_1 and p_2, as the transfer function,

$$H(\omega)=\frac{p_1(\omega)}{p_2(\omega)}, \qquad [2.18]$$

Equation 2.17 can, be rearranged, and written as

$$Z_M(\omega)=\frac{i\omega\rho d_{12}}{2}\frac{[H(\omega)+1]}{[1-H(\omega)]}. \qquad [2.19]$$

The substitution of p_1 and p_2 with the transfer function is made since this is a function that is well defined in spectral analysis, and is readily available in most data acquisition systems.

Allard and Seiben go further. Assuming plane waves, the impedance at the measurement plane, Z_M, can be used to calculate the impedance of the SOFI surface, Z_0,

$$Z_0=\frac{\left[Z_M-i\rho c\tan\left(\frac{\omega d}{c}\right)\right]}{\left[\rho c-iZ_M\tan\left(\frac{\omega d}{c}\right)\right]}. \qquad [2.20]$$

where d is the distance from the measurement plane to the SOFI surface.

Because the microphones are placed close to each other relative to a wavelength, the impedance measurement is sensitive to phase differences [Fahy]. Small errors in the measured phase between the microphones can be introduced by the phase errors between the two microphone channels which will cause the transfer function to be incorrect. The effect of the errors must be minimized through the calibration process. Chapter 3 will detail this process and the other issues involved with making impedance measurements as well as the physical setup required for the measurements.

CHAPTER 3. IMPLEMENTATION AND EXPERIMENTAL SETUP

This chapter will detail the specific equipment used to make the impedance measurement, including the equipment used to generate the noise that was measured to determine the impedance, the equipment used to measure the impedance, and the calibration of the impedance measurement equipment. The physical setup required for each experiment will also be described.

3.1 Electronic Equipment

The electronic equipment for the measurement remained the same for all experiments. The electronic equipment was divided into equipment that generated noise and equipment used to measure impedance.

3.1.1 Equipment used to generate noise

Figure 3.1 shows a block diagram of the equipment used to generate noise for the impedance measurement. The first step in generating the noise was to create a broadband random signal. This was as done through a random noise generator, General Radio Co.

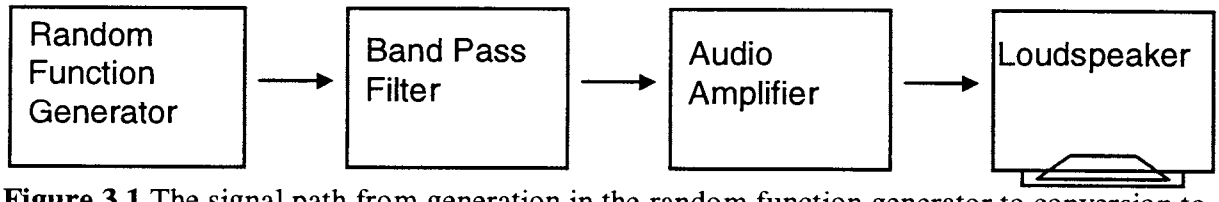

Figure 3.1 The signal path from generation in the random function generator to conversion to audible sound at the loudspeaker.

Type 1390-A, which was set to generate random noise from 0 to 20,000 Hz. This noise was then passed through a band-pass filter, Krohn-Hite model 3550, which was set to cut offs of 500 Hz and 7,000 Hz. The decision to use these frequencies for the band-pass filter was made after some initial data was taken without the band-pass filter present. The initial measurements showed that the impedance measurement did not produce useful information below 500 Hz. This conclusion was reached after comparing several initial measurements and discovering that the frequency range from 0 to 500 Hz was identical in all of the measurements. The decision to use 7,000 Hz as the high frequency cut-off for the band-pass filter was reached based on the maximum sampling rate of 18,000 Hz that was used for all the measurements. This produces a Nyquist frequency of 9,000 Hz. In order to have the noise cut off at 9,000 Hz the upper frequency limit of 7,000 Hz was used, due to the fact that the filter drop off above the high frequency cut-off is gradual.

This filtered random signal was then passed to an audio amplifier, Bruel and Kjaer Type 2706. The audio amplifier was adjusted to the highest volume possible, while avoiding clipping of the signal. Once the signal was amplified to the power required, it was fed into an 8 inch loudspeaker. The loudspeaker was housed inside a sealed enclosure made of ¾" plywood.

3.1.2 Equipment used to measure impedance

Figure 3.2 shows a block diagram of the equipment used to measure impedance. The signal path for the measurement of impedance starts in the microphone tip. The microphone tip output is a small voltage signal that must then be run through the microphone preamplifier. Figure 3.3 shows the microphone tip detached from the preamplifier. The microphones were both Bruel and Kjaer type 4939 microphones with sequential serial numbers 2389726 and 2389727. Microphones with sequential serial numbers are likely to have only small phase differences.

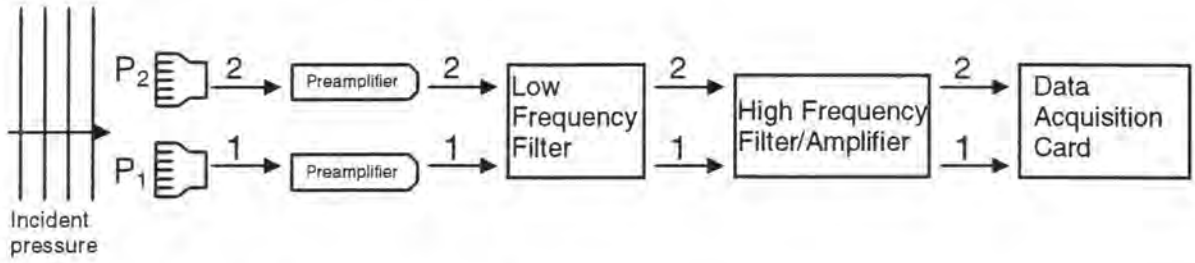

Figure 3.2 The path of the signal from detection to acquisition.

The signal is then passed into the high-pass filter, Ithaco S30. The purpose of the high-pass filter is to remove any signals below 100 Hz to minimize ground loop noise. After the high-pass filter the signal was run into the low-pass filter, Stanford Research Systems Inc. model SR640, where it was amplified to around two volts. In the low-pass filter the signal was also filtered at 9000 Hz, corresponding to the Nyquist frequency of the 18000 Hz sampling rate. This filtering was done to avoid aliasing. The amplification was done so that the data acquisition card would have good resolution on the incoming signal. The magnitude of amplification required to produce an output signal of two volts was 40 dB in free field measurements and 20 dB during the impedance tube measurements. The signal was then input to a data acquisition card, National Instruments DT 2801, installed in a PC. A program written in LabView was used to control the acquisition of the data and data storage. At each measurement point, the LabView program stored the raw time signals from each microphone.

The only step on this process which is widely accepted not to induce a phase difference into the signal is the microphone preamplifier step.

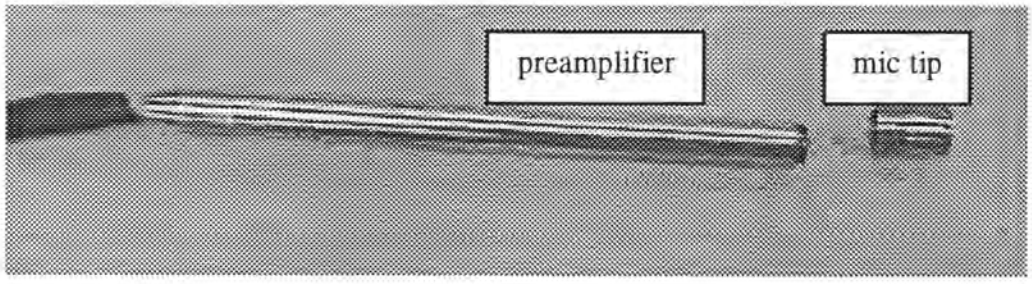

Figure 3.3 Microphone preamplifier and tip

The transfer function between the two microphones, $H(\omega)$, that is needed to calculate the impedance with Equation 2.18 is calculated in the data acquisition program as

$$H(\omega)=\frac{G_{P_1P_2}(\omega)}{\sqrt{G_{P_1P_1}(\omega)}} \quad [3.1]$$

where the auto spectrum of the first microphone signal is

$$G_{P_1P_1}(\omega)=P_1(\omega)P_1^*(\omega) \quad [3.2]$$

and the cross spectrum of the two microphone signals is

$$G_{P_1P_2}(\omega)=P_1(\omega)P_2^*(\omega) \quad [3.3]$$

where * denotes the complex conjugate. The voltage measured by the data acquisition card is used to determine pressure. However the signal recorded by the data acquisition card was voltage $V(\omega)$, with the form

$$V(\omega)=P(\omega)H_{eqpt}(\omega)H_{mic}(\omega), \quad [3.4]$$

where $H_{mic}(\omega)$ is the transfer function of the microphones and $H_{eqpt}(\omega)$ is the transfer function of the other equipment in the measurement system, $P(\omega)$ is the actual pressure and ω is the circular frequency. In order to obtain pressure for the impedance measurement the microphone and equipment transfer functions, $H_{mic}(\omega)$and $H_{eqpt}(\omega)$, must be determined so that they are removed. This will be done through the process of calibration.

3.2 Calibration

As shown in equation 3.4, when the measurements are performed the voltages are recorded. The transfer functions of both the microphones and the other equipment must be eliminated. The transfer functions are assumed to have the forms

$$H_{eqpt}(\omega)=\left|H_{eqpt}\right|e^{j\phi_{eqpt}(\omega)} \quad [3.5]$$

and

$$H_{mic}(\omega)=\left|H_{mic}\right|e^{j\phi_{mic}(\omega)}. \quad [3.6]$$

The magnitude, $|H_{eqpt}|$, is assumed to be 1. If the phase errors, ϕ_{mic} and ϕ_{eqpt}, are combined

$$\phi_{error}(\omega) = \phi_{mic}(\omega) + \phi_{eqpt}(\omega). \quad [3.6]$$

Then when a measurement is taken, the cross spectrum between the voltage signals from each microphone, $G_{V_1V_2}$, is calculated

$$G_{V_1V_2}(\omega) = V_1(\omega)V_2^*(\omega) = P_1(\omega)P_2^*(\omega)|H_1||H_2|e^{j(\phi_{error}(\omega))} \quad [3.7]$$

where, V_1 and V_2 are the voltages measured by the data acquisition card. $|H_1|$ and $|H_2|$ are the magnitudes of the transfer functions from each of the microphone channels, and ϕ_{error} is the phase angle introduced by all of the electronic equipment. Then to find the cross-spectra, $G_{P_1P_2}$, of the pressures we must take

$$G_{P_1P_2}(\omega) = P_1(\omega)P_2^*(\omega) = G_{V_1V_2}(\omega)\frac{e^{-j(\phi_{mic}(\omega)+\phi_{eqpt}(\omega))}}{|H_1||H_2|}. \quad [3.8]$$

To calculate $G_{P_1P_2}$ the desired quantity, the equipment errors, ϕ_{mic}, ϕ_{eqpt}, $|H_1|$, and $|H_2|$ must first be calculated so that their error can be compensated for. Determining ϕ_{error} will be called phase calibration and determining $|H_1|$ and $|H_2|$ will be called magnitude calibration.

3.2.1 Phase calibration

There are two main sources of phase error, first the phase error induced by the microphone tips, ϕ_{mic}, and second the phase error introduced by the filter, amplifier and data acquisition card, ϕ_{eqpt}. Each of these phase errors will be corrected separately. Further, the phase error must also be calculated separately for each sampling rate, because there are non-linear effects of changing sampling rate on phase error introduced by the data acquisition card.

Phase calibration of the filter/amplifier system, ϕ_{eqpt}, was done by calibrating the entire amplifier filter system at one time. This calibration process will calibrate for the phase error introduced by the low frequency filter, the high frequency filter and amplifier, and the data acquisition card. The signal from a single microphone was fed into both channels of the filter/amplifier system. The phase difference between the two signals was taken to be the

phase error introduced by the filter/amplifier system since a perfect system would have no phase difference due to the fact that the inputs to both channels were identical. A typical equipment phase error is shown in Figure 3.4. Since the phase error between 8000 and 9000 Hz is so widely varying, results in this frequency range should be ignored.

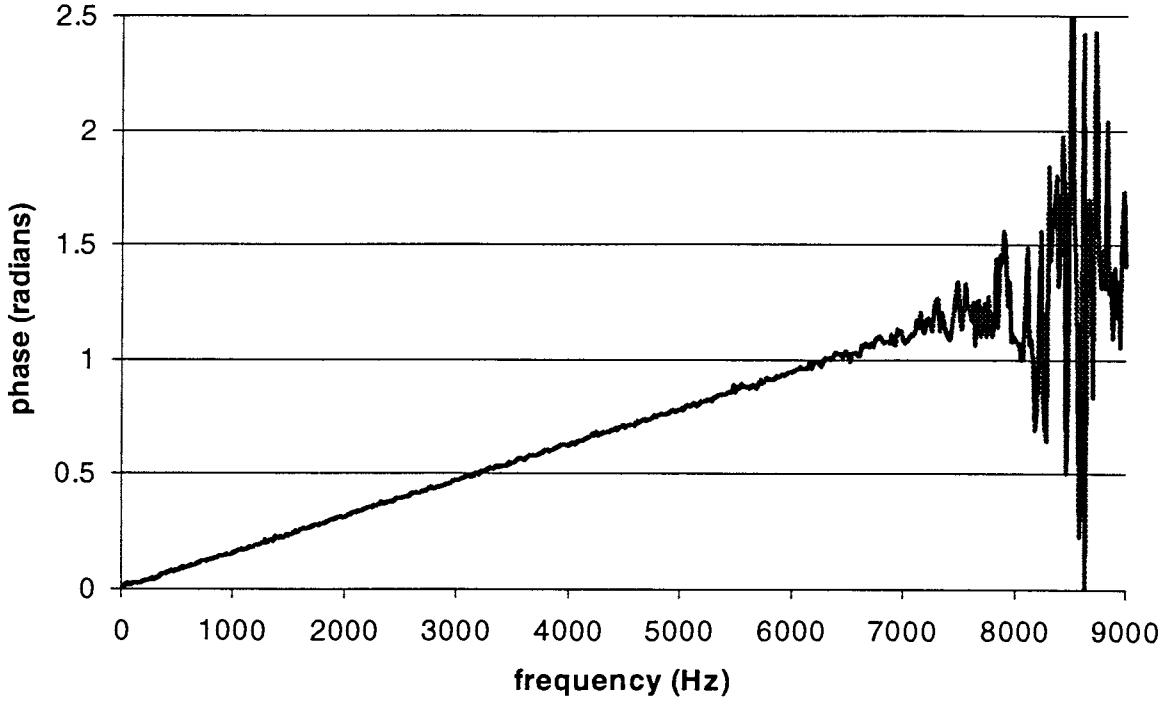

Figure 3.4 A typical phase calibration error for the equipment.

Now that ϕ_{eqpt} is known and has been eliminated from Equation 3.7, the following tests can be used to calculate ϕ_{mic}. Both tests were done with the microphones placed horizontally at the same height in the holder above a simple sound source as in Figure 3.5. The first test was with the microphone tips on the normal preamplifier as in Figure 3.6a. In the second test the microphone tips were switched to the opposite preamplifier as in Figure 3.6b. Using these two tests the phase difference was calculated between the two microphones based on the assumption is that the pressure at each location remains the same. This means that from the two tests a measurement is taken of the same pressure, the only difference being which microphone tip did the measuring.

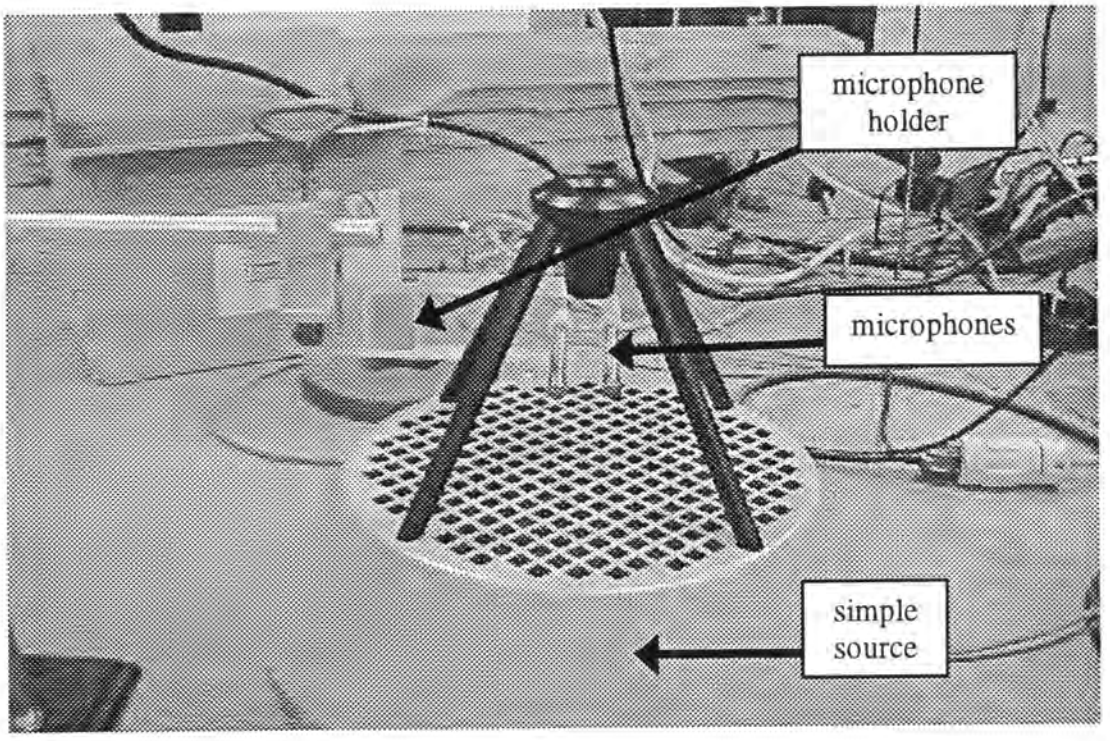

Figure 3.5 Microphones in place above a simple sound source for the microphone tip calibration.

For the first test,

$$V_1(\omega) = P_1(\omega) H_{mic1}(\omega) \qquad [3.9]$$

and

$$V_2(\omega) = P_2(\omega) H_{mic2}(\omega). \qquad [3.10]$$

The microphone transfer function of a microphone H_{mic} is given by

$$H_{mic}(\omega) = |H_{mic}| e^{j\phi_{mic}(\omega)}. \qquad [3.11]$$

Then for each microphone

$$H_{mic1}(\omega) = |H_1| e^{j\phi_{mic1}(\omega)} \qquad [3.12]$$

and

$$H_{mic2}(\omega) = |H_2| e^{j\phi_{mic2}(\omega)}. \qquad [3.13]$$

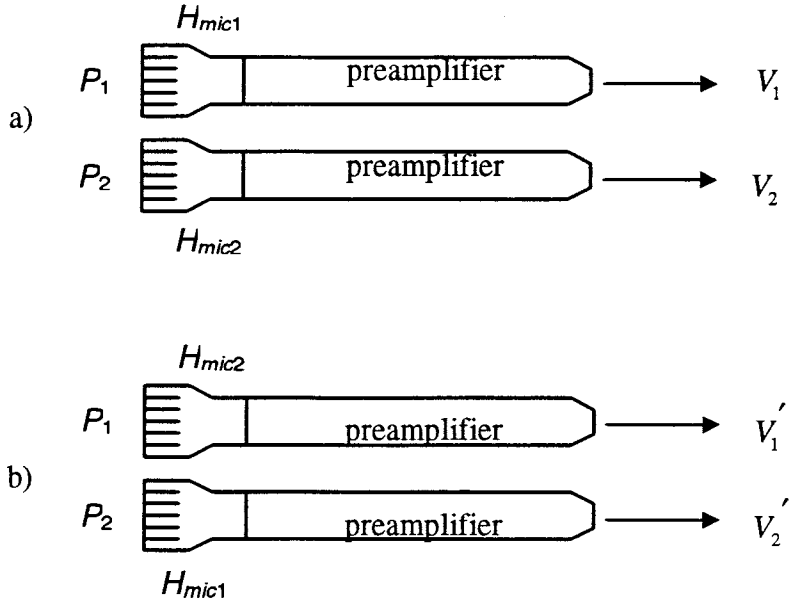

Figure 3.6 Depiction of microphones during the calibration tests.
a) Microphones during the first test with the tips on the original preamplifiers.
b) Microphones during the second test with the tips on the opposite preamplifiers.

From the second test

$$V_1'(\omega) = P_1(\omega)H_{mic2}(\omega) \qquad [3.14]$$

and

$$V_2'(\omega) = P_2(\omega)H_{mic1}(\omega). \qquad [3.15]$$

The cross-spectrum of V_1 and V_2 is then calculated

$$G_{V_1V_2}(\omega) = V_1(\omega)V_2^*(\omega) = P_1(\omega)P_2^*(\omega)|H_1||H_2|e^{j(\phi_{mic1}(\omega)-\phi_{mic2}(\omega))} \qquad [3.16]$$

where V_2^* is the complex conjugate of V_2 and P_2^* is the complex conjugate of P_2. The cross-spectrum of V_1' and V_2' is

$$G_{V_1'V_2'}(\omega) = V_1'(\omega)V_2'^*(\omega) = P_1(\omega)P_2^*(\omega)|H_1||H_2|e^{j(\phi_{mic2}(\omega)-\phi_{mic1}(\omega))} \qquad [3.17]$$

so then if the 2 cross-spectra are divided

$$\frac{G_{V_1V_2}(\omega)}{G_{V_1'V_2'}(\omega)} = e^{2j(\phi_{mic1}(\omega)-\phi_{mic2}(\omega))}. \qquad [3.18]$$

Since $\phi_{mic} = \phi_{mic2} - \phi_{mic1}$, then the phase error, ϕ_{mic}, is

$$\phi_{mic}(\omega) = \frac{1}{2} angle\left(\frac{G_{V_1V_2}(\omega)}{G_{V_1'V_2'}(\omega)}\right). \qquad [3.19]$$

A typical phase error introduced by the microphone tips is shown in Figure 3.7.

Once this calibration of the error angle introduced by the microphones ϕ_{mic} and the equipment ϕ_{eqpt} are determined, the phase calibrated cross-spectra is

$$\left(G_{V_1V_2}(\omega)\right)_{cal} = \left(G_{V_1V_2}(\omega)\right)_{meas} e^{-j(\phi_{mic}(\omega)+\phi_{eqpt}(\omega))}. \qquad [3.20]$$

This phase calibrated cross-spectra is used to get the correct transfer function from microphone 1 to microphone 2.

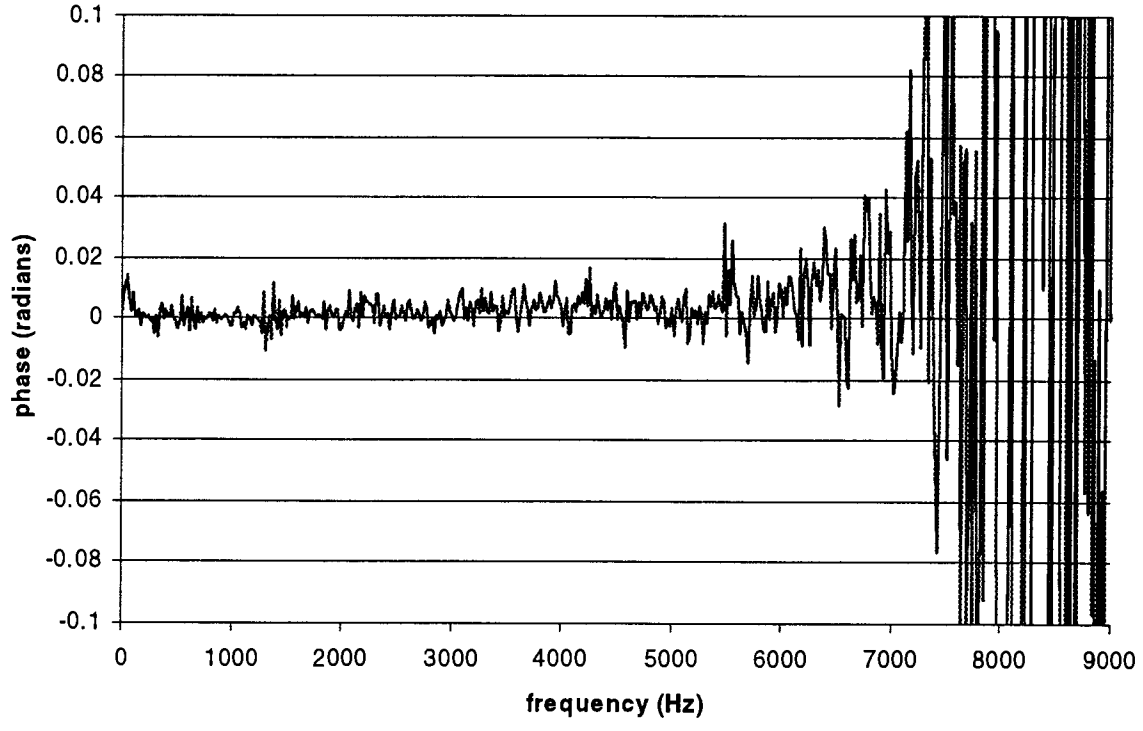

Figure 3.7 A typical phase error for the microphone tips.

3.2.2 Magnitude calibration

The amplitude calibration factor, $|H|$, was found by recording a sample from each microphone exposed to a calibrated noise source. Since the calibrated noise source has a known magnitude at a known frequency, then the value of $|H|$ is directly calculated. Each microphone was calibrated separately. First, the Fourier Transform of the time signal is calculated and the auto-spectrum of the channel being magnitude calibrated is calculated. Then, the auto-spectra is summed over points near the peak of the calibrated noise source. For this case the calibrated noise source output was 94 dB at 1000 Hz, so the sum, *sum*, was taken from 900 Hz. to 1100 Hz. Then,

$$|H| = \frac{\sqrt{\frac{sum}{10^{\frac{94}{10}}}}}{20\times10^{-6}}. \qquad [3.21]$$

The square root must be taken because the auto-spectrum is the spectrum magnitude squared and the factor of $20\text{x}10^{-6}$ is a standard reference value used for sound pressure levels.

3.3 Physical Equipment Setup

This section will detail the physical equipment setup used for each experiment. Certain equipment was used for all tests; the holder developed for the SOFI panel, the support for the microphone holder, the microphone holder and the microphones themselves. Other aspects of the physical setup that were designed for each individual experiment include, the in room stand, the reverberant room environment, the box stand, the anechoic chamber, and the impedance tube setup.

One of the issues with the sample that was received from NASA was its small size. The sample is 22 inches by 22inches. This creates a potential problem that edge reflections can pose a significant problem to acoustic impedance measurements. To solve this problem a stand and baffle was built for the SOFI sample, Figure 3.8. The stand used for holding the

SOFI sample was the same for all the experiments. The stand was made to provide a reflection surface that would fit snugly around the SOFI sample and prevent reflections around the edge of the SOFI sample. The SOFI sample was mounted in a wood frame constructed with 2 inch by 4 inch pine with a ¾ inch medium density fiberboard (MDF) baffle. The 4 foot by 4 foot MDF baffle had a hole cut in the center to fit the SOFI sample tightly. This size should prevent edge reflections from being an issue when taking measurements close to the center of the baffle. The SOFI sample was mounted in the stand so that the surface of the SOFI was flush with the surface of the baffle. While the SOFI sample was mounted flush with the surface of the baffle it was not allowed to rest on the wood frame.

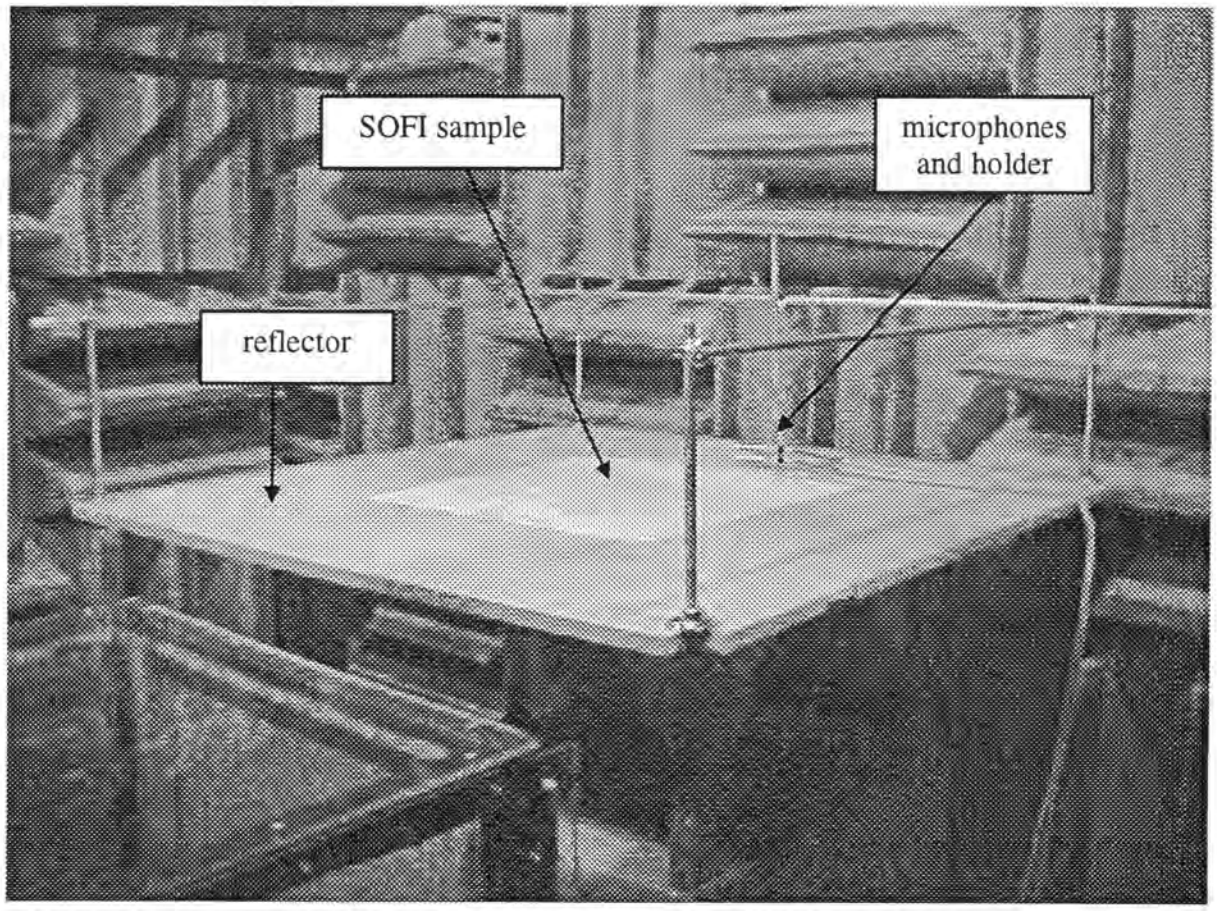

Figure 3.8 Frame and baffle used to support the NASA SOFI sample. The photo was taken in the anechoic chamber.

The concern was that if the aluminum plate backing of the SOFI sample rested directly on the wood frame, it would rattle when subjected to the high noise levels, from 80 to 85 dB, required for the impedance measurement. To prevent the rattling of the aluminum on the wood a layer of polyethylene foam was inserted between the plate and the stand. Care was taken to ensure that even with the polyethylene foam inserted, the surface of the NASA SOFI sample would be nearly flush with the surface of the baffle.

As can be seen in Figure 3.6, once the stand was built, aluminum rods were attached to hold the microphones. This allows the microphones to be positioned anywhere in 3 dimensions over the SOFI sample. A measurement plane height of 2.5 cm. above the SOFI surface was chosen for the microphones as the closest possible distance. All measurements were done at this height.

The microphone holder was used to keep the microphones in a consistent orientation relative to each other. The holes for the microphones are 2 cm. from center to center. The holder was made out of Plexiglas for ease of fabrication and duplication. There is a mark on the side of the holder denoting the midpoint of the line between the centers of the two holes for the microphones, this was the line used for determining the height of the measurement plane. The measurement plane was measured at the beginning of testing every day and was measured at various times during testing.

3.3.1 Anechoic chamber experiment

The experiment in the anechoic chamber was done first; this was to provide an environment that was free of outside noise sources and reflections so the focus would be on obtaining clean results from the impedance analysis. The anechoic chamber has a 12 foot by 12 foot by 10 foot dimension, and is anechoic to around 250 Hz. There was equipment present in the chamber for other unrelated research, but the baffle surface was kept higher than the other surfaces; so that there would be no reflection off of the other setup that entered the measurement area. The speaker was positioned over the center of the SOFI sample at a height of 46.5 inches, Figure 3.9. Also visible in Figure 3.9 are the fiberglass wedges in the chamber walls that are responsible for absorbing the acoustic energy incident on the walls.

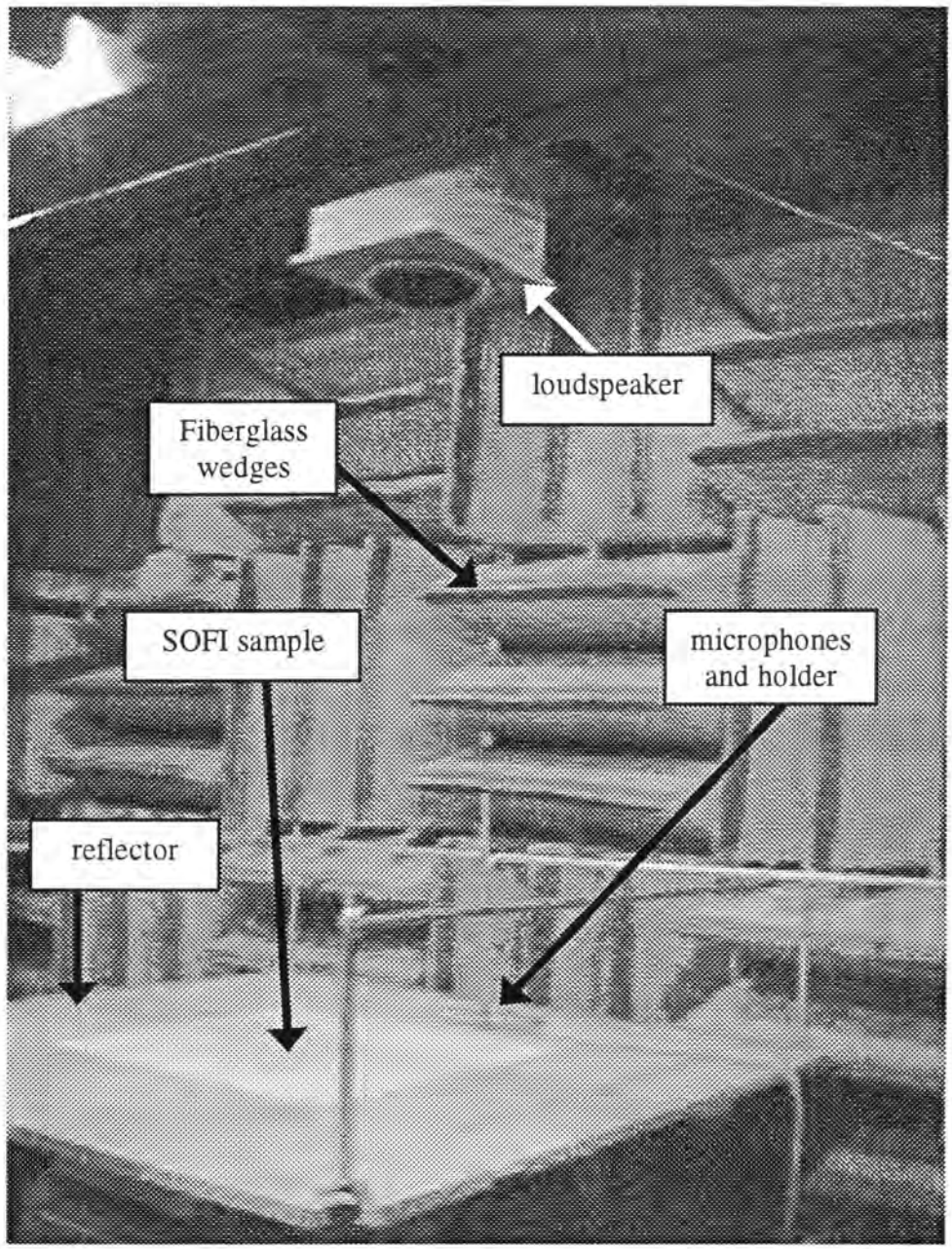

Figure 3.9 Test setup in the anechoic chamber.

3.3.2 Reverberant room experiment

This experiment was done in the lab environment which is a large room with concrete walls, floor and ceiling. The open ceiling houses ductwork, pipes and electrical connections, while the floor features an open tank filled with water and a large depression for the anechoic

chamber. Two walls are lined with counters and cabinets of wood, glass and Formica. During experiments there was background noise from other experiments, people talking, and the ventilation system. Also, surrounding equipment and fixtures were typically moved between measurements, so the acoustic reflectors were not consistent between measurements.

The same mount was used to hold the SOFI in place and the mount was simply placed on the floor. A frame was built to hold the speaker above the SOFI mount. For convenience, the frame was mounted on an anti-vibration pad built into the floor. The frame was constructed out of uni-strut and is shown in Figure 3.10. Once the frame was in place, the

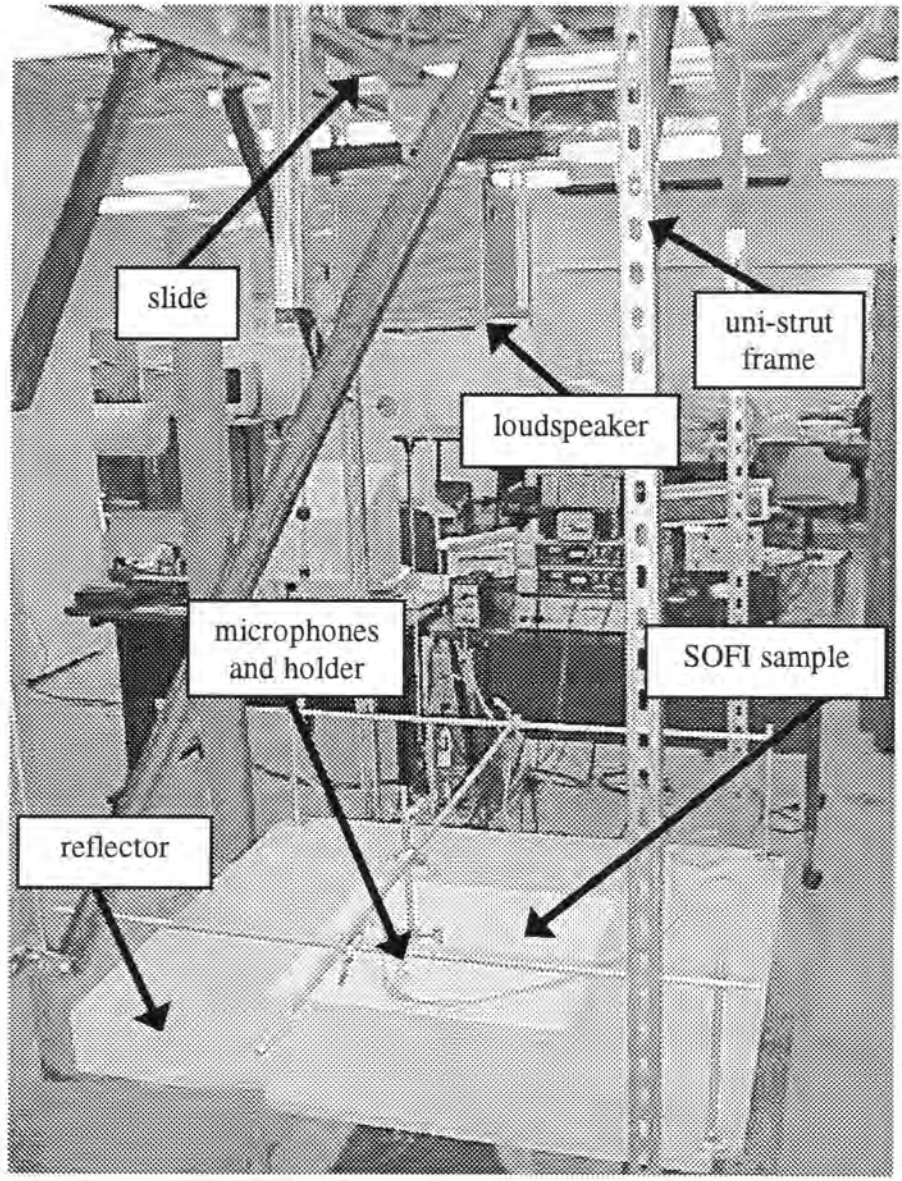

Figure 3.10 The stand built in the reverberant room.

speaker was mounted on a slide in the frame. The slide was adjustable vertically to position the speaker at different heights and the slid allowed the speaker to move back and forth horizontally. To accomplish the third degree of freedom, the SOFI mount could be moved back and forth on the floor. With this frame built to hold the speaker, the speaker was positioned at the same height of 46.5 inches above the SOFI surface as it was inside the anechoic chamber.

3.3.3 Moving source experiment

The goal of the experiment with the moving source was to test whether the relationship between the microphone holder and the speaker effects the measurements. To accomplish this, the relationship between the speaker and the microphones was set to be the relationship between the speaker and the microphones at location 10, which is 5 inches from the edge of the SOFI and over the center of the cut, this arrangement is shown in Figure 3.11. This location was chosen because the speaker is directly over the microphone tips when they

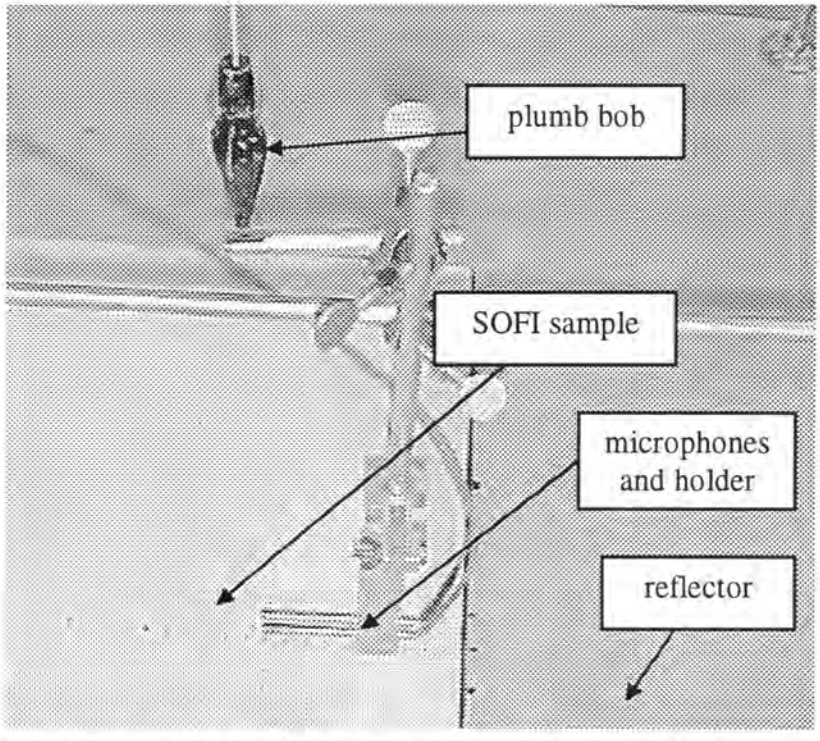

Figure 3.11 The microphone holder as it is being aligned with the speaker before a measurement for location 10.

are in this position. Since the speaker is mounted on a slide in the reverberant room setup moving the speaker could be readily moved across the SOFI sample as the measurement was done at different points. To do the perpendicular set of measurements, the panel was rotated in its holder ninety degrees. To guarantee that the speaker and microphone holder had the same relationship at each measurement, an aluminum rod was mounted to the microphone holder with a red dot on it. A plumb bob was hung from a pre-existing hole in the speaker box and aligned with the red dot on the aluminum rod before each measurement.

3.3.4 Impedance tube experiment

The impedance tube experiment is an attempt to provide a better environment for measuring the impedance of the SOFI, while remaining in the reverberant room. The basic setup for the impedance tube experiment is that a frame was built around the loudspeaker and a tube was mounted to the frame. The microphones were then placed in the tube flush with the inside wall. This positioning does several things for the measurement. First, in the previous measurements it was simply assumed that since the microphones were far away from the source the spherical waves that were emitted by the source were approximately plane waves at the surface of the material. However, in the tube plane waves are guaranteed up to a frequency with a half wavelength of the diameter of the tube. Second, the tube isolates the microphones from the environment. This is not perfect isolation but it is better than making a measurement in the free field with other noise sources present. Figure 3.12a shows the concept of the impedance tube and Figure 3.12b shows how the concept was implemented, while Figure 3.13 shows how the impedance tube was used during a measurement.

The tube had an internal diameter of 1 inch, which guaranteed plane waves in the tube up to 6750 Hz. This was considered sufficient because the phenomena studied in the previous experiments have had frequencies between 2000 and 3000 Hz. Several lengths of tubes were used to determine if the length of the tube would effect the measurement of the impedance at the frequency which was determined to be of interest. The chosen lengths were 15 inches,

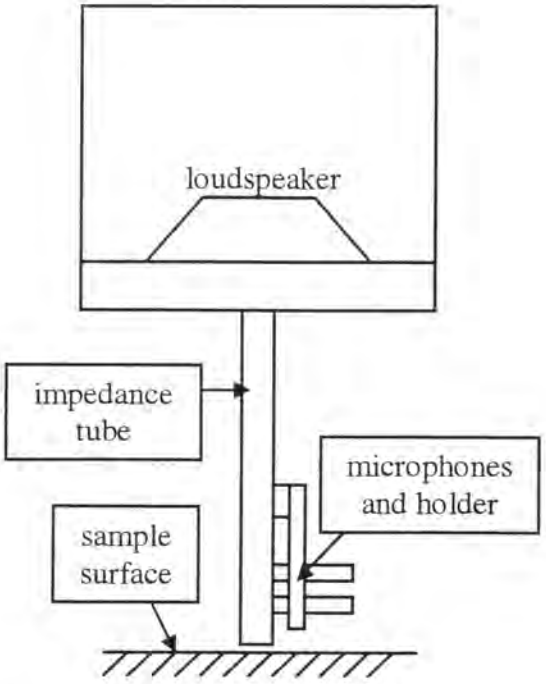

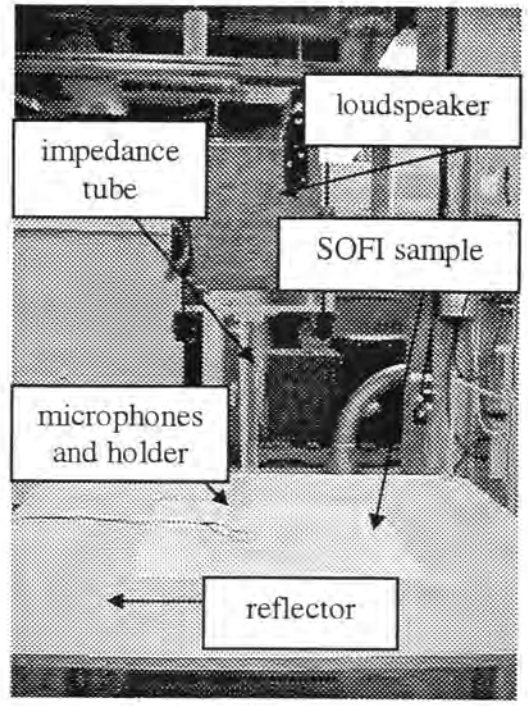

Figure 3.12 a) The impedance tube concept. b) The impedance tube implementation

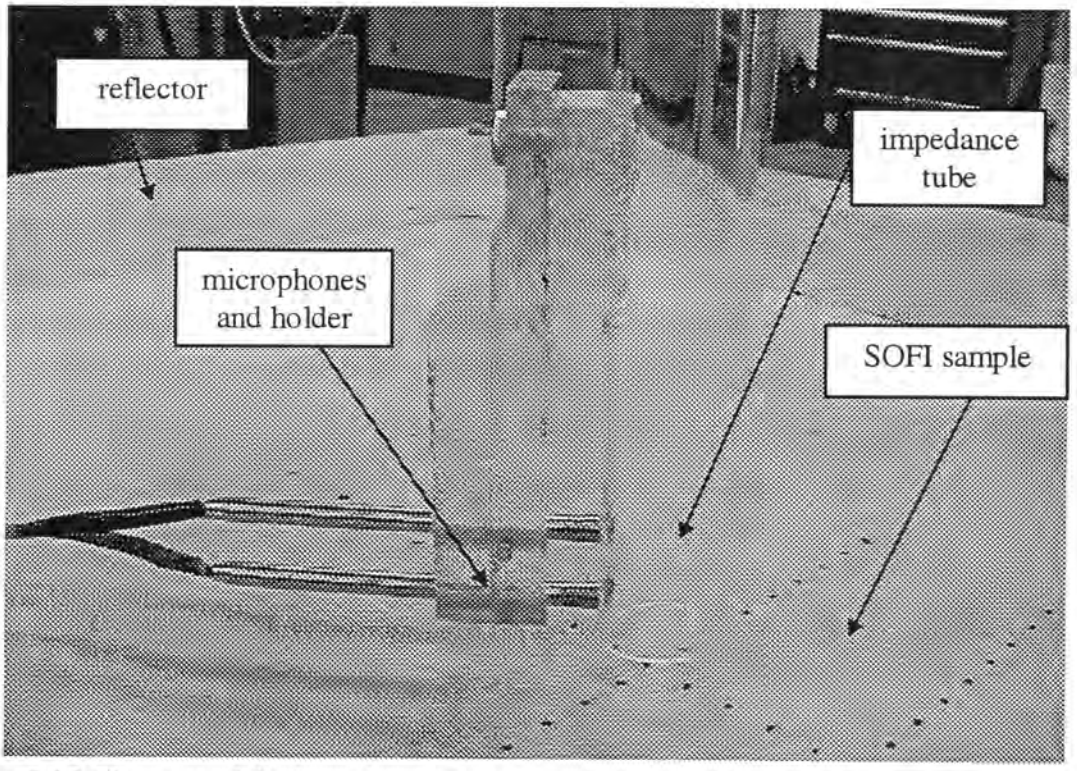

Figure 3.13 Close up of the impedance tube measurement in situation to measure location 10.

16.5 inches and 18 inches. These lengths were chosen based on the frequencies of 2650 Hz and 2450 Hz, which were the frequencies of interest identified in previous experiments. These frequencies correspond to wavelengths of 5.5 inches and 5 inches respectively. Therefore the 15 inches and 16.5 inch long tubes would be on resonance for both frequencies and the 18 inch tube would be off resonance for both frequencies.

Figure 3.13 shows the impedance tube during a measurement. The microphones are mounted so that their faces are flush with the inside wall of the tube. The height of the measurement plane, midpoint of the two microphones, was 2.5 cm for this experiment as it was for the other experiments. The tube opening was held approximately 7 mm about the SOFI surface.

CHAPTER 4. RESULTS

Once the calibration system was setup and the data processing programs were written, a measurement was taken of a calibrated sound source. This result was compared with known results for the impedance of a calibrated sound source [Mann]. This showed that the programs and measurement system were working as expected and producing reliable results for the measurement of both the real and imaginary parts of impedance.

The SOFI sample was received with a small cut on one side; this cut was one inch by five inches. Some initial measurements were made comparing this location to a symmetric location on the sample where it was assumed that the SOFI was well bonded to the metal. These results only showed that some differences could be determined between the bonded and un-bonded regions. Viewing the results from this initial test, there was concern that the cut that was initially made in the sample was not far enough from the edge of the SOFI sample to ensure that the edge was not influencing the results. Another concern was the 1 inch width of the cut, which is small compared to the wavelength of acoustic energy incident on the SOFI in that area. Because it was only one inch wide, this initial cut may not have been readily visible in the impedance measurements. For these reasons a second cut was made. The second cut was two inches wide and eight inches long. This new cut had more than three times the area of the initial cut and showed much clearer differences between it and the un-bonded areas. This discussion of results will be focused on the second cut.

Because the impedance measurements can vary widely over several orders of magnitude, it is not convenient to use a linear scale to examine the impedance. Three scales were used to examine impedance. First is a dB scale,

$$Z(dB) = 10\log_{10}(Z), \qquad [4.1]$$

which gives the impedance relative to 1. Since he factor ρc is common in acoustics and in impedance measurements, a second scale reported the impedance in dB relative to ρc,

$$Z(dBrel\rho c) = 10\log_{10}\left(\frac{Z}{\rho c}\right). \qquad [4.2]$$

The final scale is dB relative to the maximum value of the impedance in the measurement area,

$$Z(dBrelMax) = Z(dB) - Max\left|Z(dB)\right|. \qquad [4.3]$$

This scale was used to compare the different indicators on similar scales.

4.1 The SOFI Sample

The SOFI sample received from NASA was 22 inches by 22 inches and 2 inches thick. The sample was backed by ¼ in thick aluminum plate. A map of the SOFI sample can be seen in Figure 4.1. The SOFI panel was built by spraying the SOFI in a line at one edge of

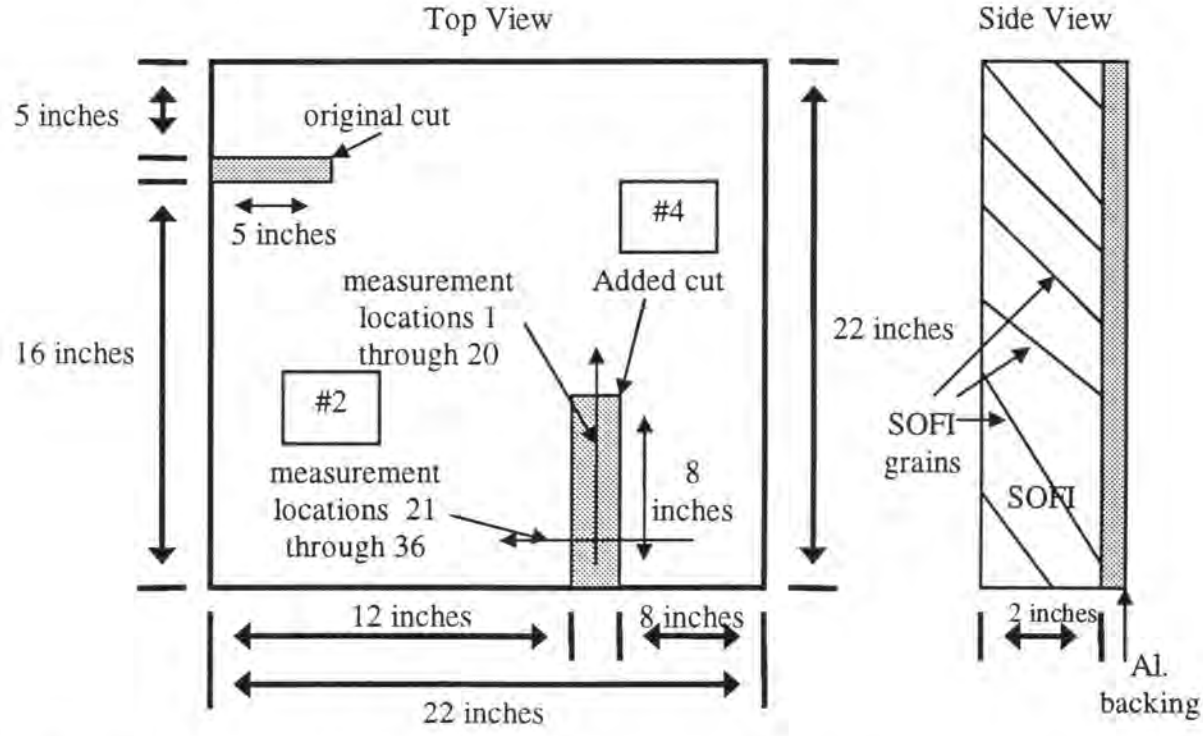

Figure 4.1 Map of the SOFI showing the location of the cuts and the measurement locations. The rectangles with #2 and #4 indicate locations where Teflon pads were inserted by NASA.

the aluminum plate, and then another line of SOFI material is laid down, overlapping the first line. This creates a diagonally layered effect in the SOFI. The layers are not all the same thickness and do not have parallel boundaries, creating a grain to the SOFI as shown in the side view in Figure 4.1. The surface of the SOFI is then smoothed off, to create a level surface.

The impedance measurements are done in two lines, which are shown in detail in Figure 4.2. The first line is down the center of the cut, starting ½ inches from the edge of the sample, and making a measurement every ½ inch. This line is numbered points 01 through 20, with point 01 being the point closest to the sample edge. The last measurement in that line, point 20, is taken 10 inches from the sample edge. The second line of measurements is taken across the cut, 2.5 inches from the edge of the SOFI sample. This distance was chosen because it will be far from the edge of the SOFI sample, and it crosses the cut where there is a well defined un-bonded area. This line is numbered points 21 through 36, with location 21 being 3 inches to the right of the cut and location 36 being 3 inches to the left of the cut. The measurements in this line were also taken on ½ inch intervals, crossing the center of the cut at location 05 on the first line, with location 28 being ½ inch to the right of the center of the cut and location 29 being ½ inch to the left of the center of the cut.

The locations on the SOFI sample map in Figure 4.1 labeled #2 and #4 are where NASA had inserted Teflon pads when the SOFI sample was manufactured, to create un-bonded areas between the SOFI and the aluminum plate. A 2 inch square Teflon pad was inserted at the location marked #2 and a 4 inch square pad was inserted at the location marked #4. The ultrasonic through-scan data from J. J. Peters and D. K. Hsu, private communication, shows that no un-bonded areas were created by the Teflon pads. Figure 4.3 shows the data from the through scan and shows good detection of the un-bonded area in the lower left corner, but detected no un-bonded areas where the Teflon pads were inserted. The wavy lines in Figure 4.3 are related to the layered nature of the SOFI. The fact that the SOFI has this layered nature also raises the possibility that there are two speeds of sound in the SOFI. One would be the speed of sound perpendicular to the SOFI surface, where the sound must cross grain boundaries, and the other would be on the diagonal parallel to the grain boundaries where the sound remains in a single grain.

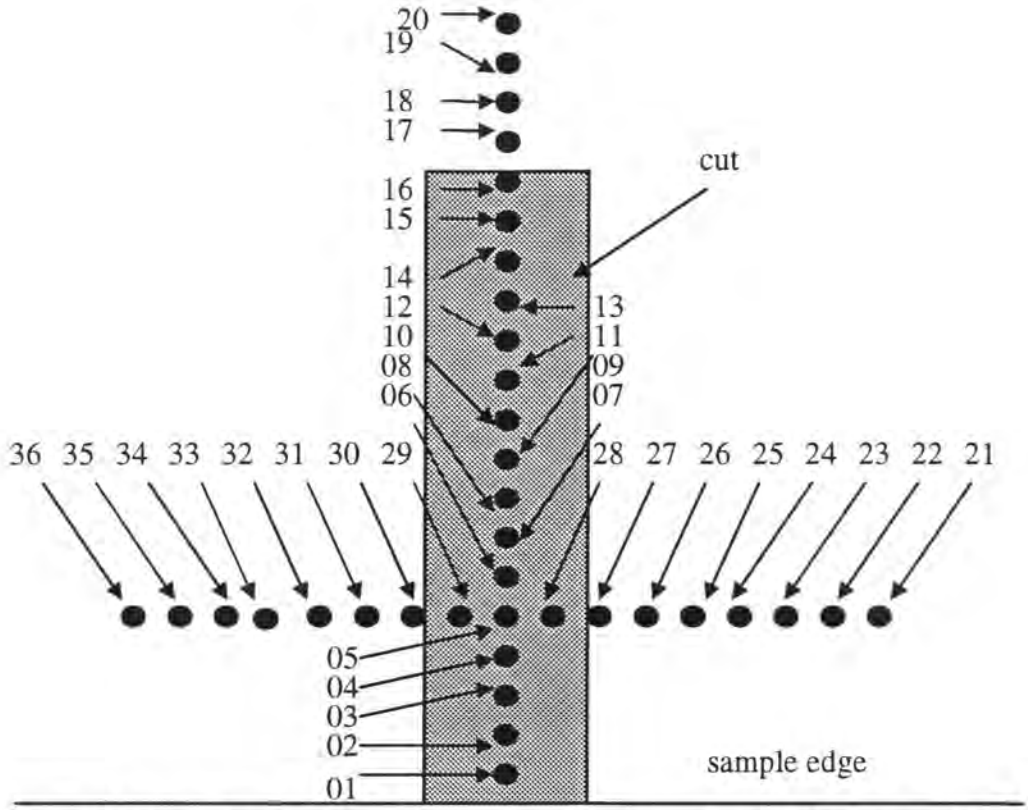

Figure 4.2 Detail showing the measurement locations, location 01 is ½ inch from the edge of the SOFI sample, the cut is 8 inches long and 2 inches wide, each measurement is ½ inch from the previous measurement.

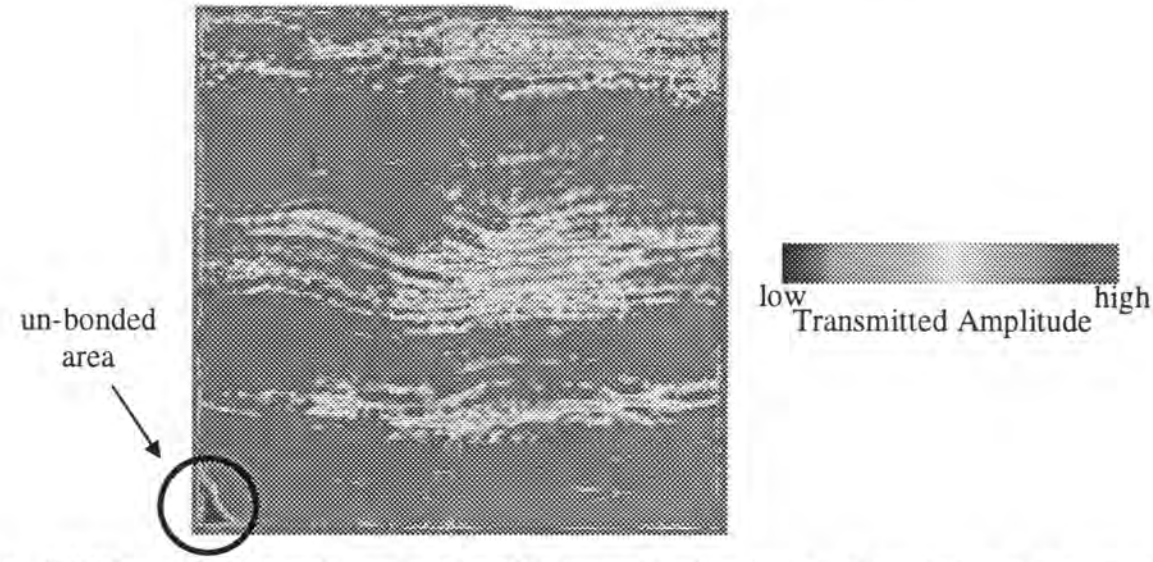

Figure 4.3 Ultrasonic Through-scan of the SOFI sample, showing an unbonded area in the corner, and no un-bonded areas at the location of the Teflon pads inserted by NASA.

4.2 Impedance Frequency Spectra

The first result that was obtained were frequency spectra of the impedance. The impedance had both real and imaginary parts, as was explained in chapter 2. The program calculated both the impedance at the measurement plan, Re(Zm) and Im(Zm), and the impedance at the SOFI surface, Re(Z) and Im(Z). An example result is shown in Figure 4.4, which was obtained from measurements taken in the anechoic chamber. Figure 4.4 also shows the problem with the impedance of the surface, Z. The measurement of the surface impedance varies widely, sometimes more than 20 dB over a very small frequency range. It also does not show differences between the measurements taken over the cut and those taken over well bonded areas. The reason for this may be that the plane wave assumption made when applying the surface impedance equation, Equation 2.20, to the measurement of the pressure was violated in this experiment. The decision was made to look only at the impedance of the measurement plane.

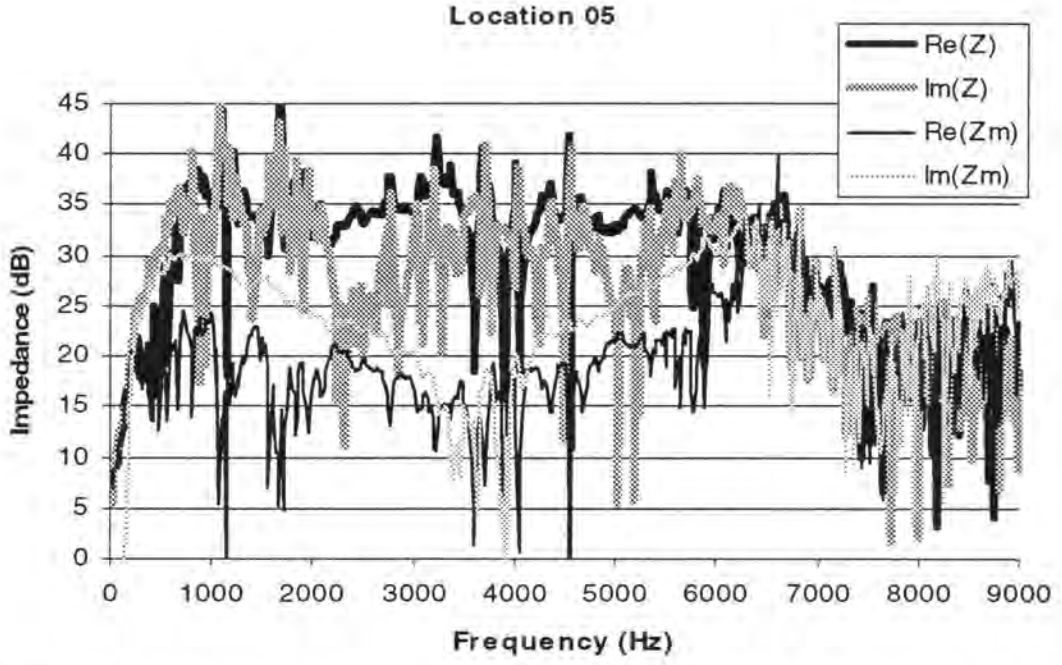

Figure 4.4 The real and imaginary parts of impedance at location 10, 5 inches in from the edge of the SOFI sample over the center of the cut.

The real part of impedance at the measurement plane is the measurement that is assumed to show differences between the bonded and cut areas. The imaginary part of impedance is related to the reactive energy, which is energy that does not propagate away from the surface of the material [Fahy], while real part of impedance is directly related to absorption which is what the bonding condition is assumed to effect. Figure 4.5 shows that the imaginary part of impedance at location 05 that is over the cut and location 36 that is 3 in. from the cut. There is no significant change over the cut. All future analysis will therefore focus on the real part of the impedance.

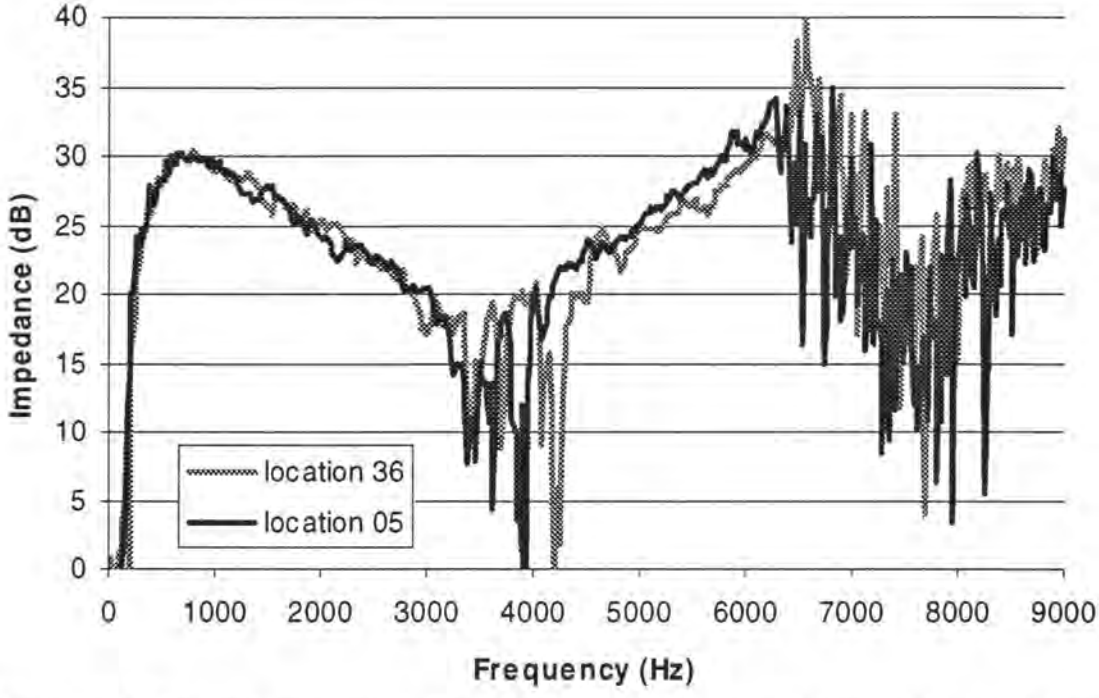

Figure 4.5 The imaginary part of impedance does not show differences between location 05, over the cut and location 36, 3 inches from the cut.

4.3 The Identified Differences in the Anechoic Chamber

Several different frequency ranges were investigated to see if differences could be identified between the impedance measurements over the bonded and un-bonded locations. Figures 4.6 to 4.9 all compare the real part of the impedance at the measurement plane for 5 locations. These locations are 21, 27, 05, 28, and 36. Location 21, which is at the right end of the line of measurements across the cut, and 36, which is at the left end of the line of measurements across the cut, are far away from the cut and locations 28, 05 and 29 are all over the cut. All of these measurement locations are 2.5 inches from the edge of the SOFI sample. Figure 4.6 shows the frequency bands that were visually identified as possibly containing differences between bonded and un-bonded locations. Figure 4.7 shows the first difference that was noted. The difference is that the real part of impedance of the bonded locations is lower near 2400 Hz than the real part of impedance of the un-bonded locations. As an alternative example, Figure 4.8 shows a close-up of the frequency range from 3000 to 4000 Hz. In this frequency range there are not dramatic differences as identified in Figure 4.7.

Based on some proof of concept measurements, it was believed that the slope of the impedance from 5000 Hz to 7000 Hz might also be an indicator of the bonding condition. However, Figure 4.9 shows that the slopes in this region are both similar from location to location and variable within the location, so this region did not make a good indicator of the bonding condition.

That a difference is found in the 2500 Hz frequency range is not unexpected. From analysis of Equation 2.13 it is found that at 2500 Hz the thickness of the SOFI corresponds to one quarter of a wavelength. This is a resonance frequency for the SOFI sample. When zero velocity is assumed at the SOFI surface a pressure node at the SOFI-aluminum interface and a velocity anti-node at the same location are the assumed conditions for a ¼ wavelength resonance. It is then expected that at the resonance of the SOFI sample the impedance should be more sensitive to the bonding condition because the measured impedance is more sensitive to the impedance at the SOFI-aluminum interface at this frequency.

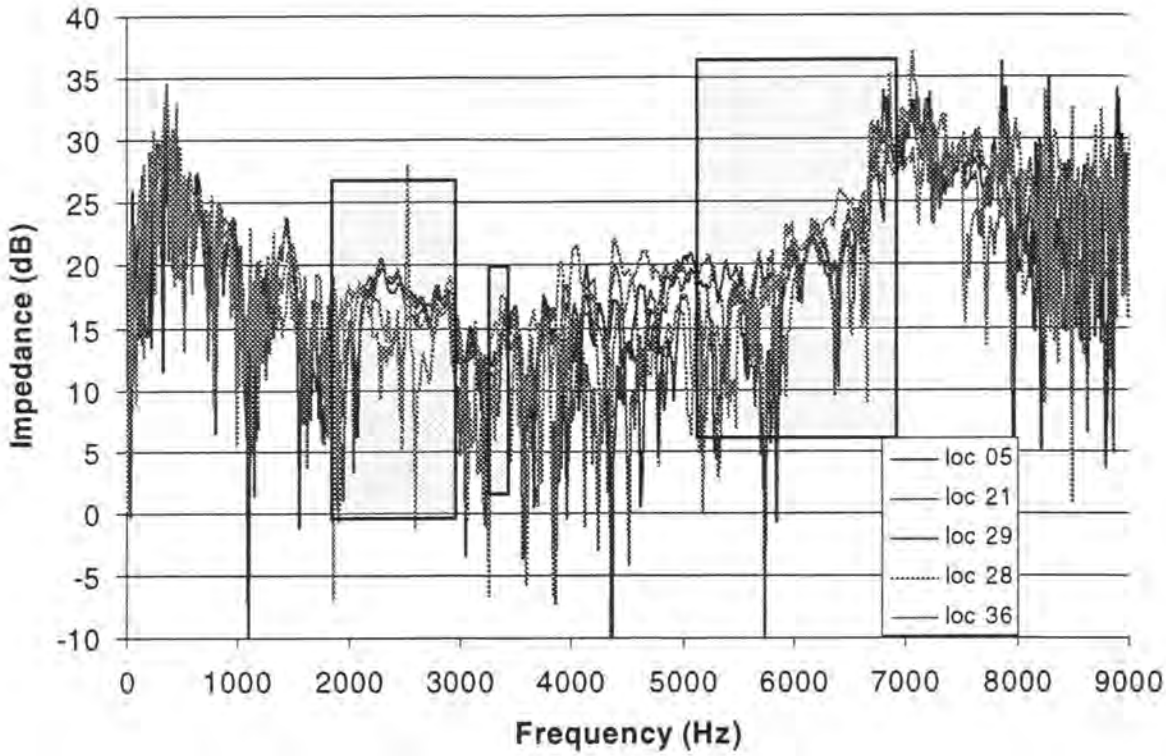

Figure 4.6 Gray boxes identify areas of possible differences in frequency spectra, between bonded and un-bonded areas.

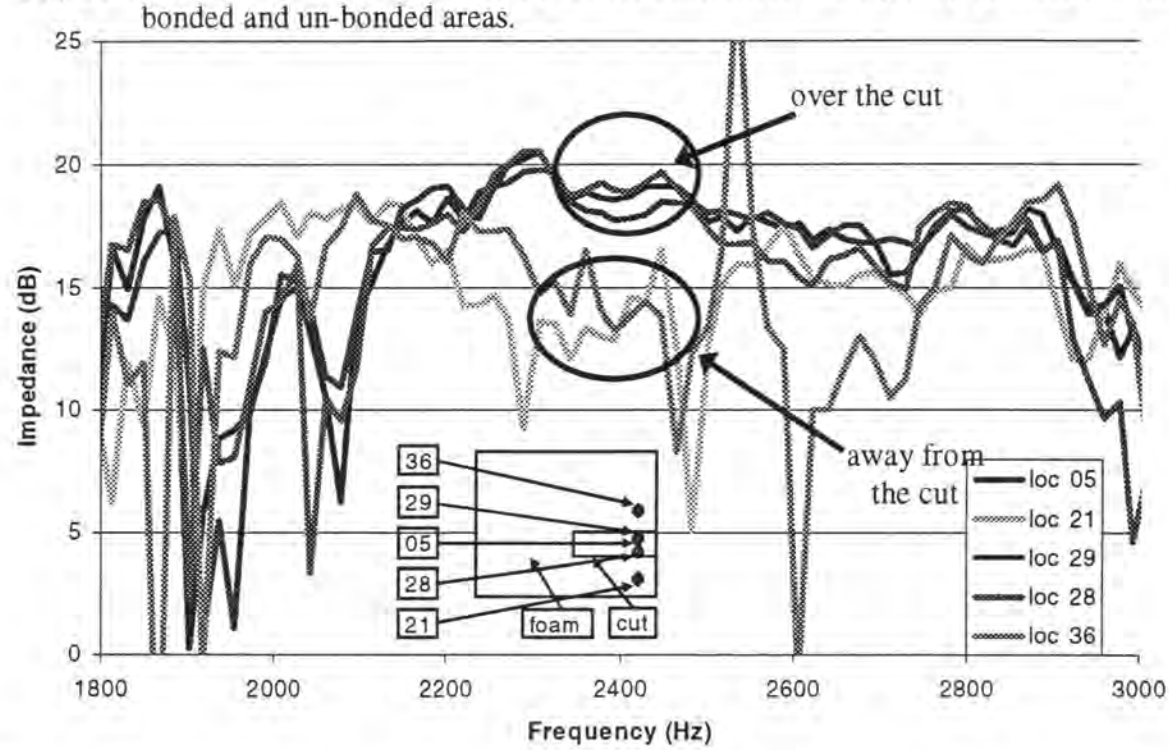

Figure 4.7 A difference in the real part of impedance was found between the bonded and un-bonded locations on closer investigation of the 1800 to 3000 Hz frequency

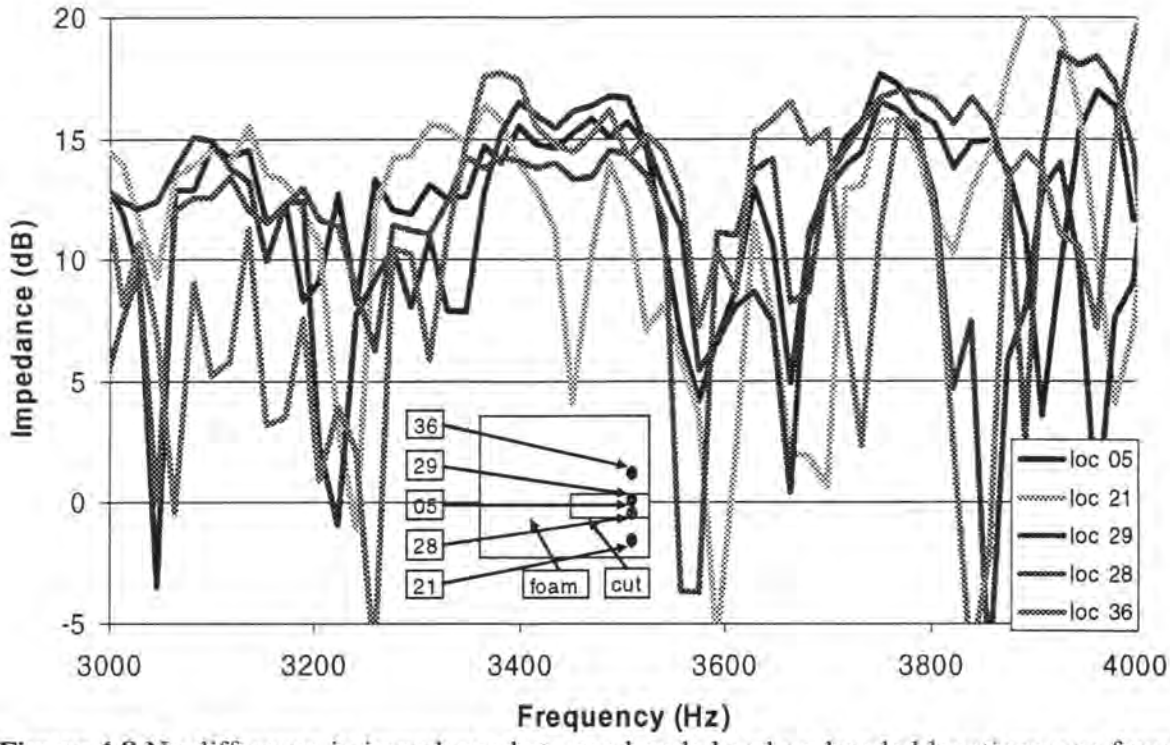

Figure 4.8 No difference in impedance between bonded and un-bonded locations was found on closer investigation of the 3000 to 4000 Hz frequency band.

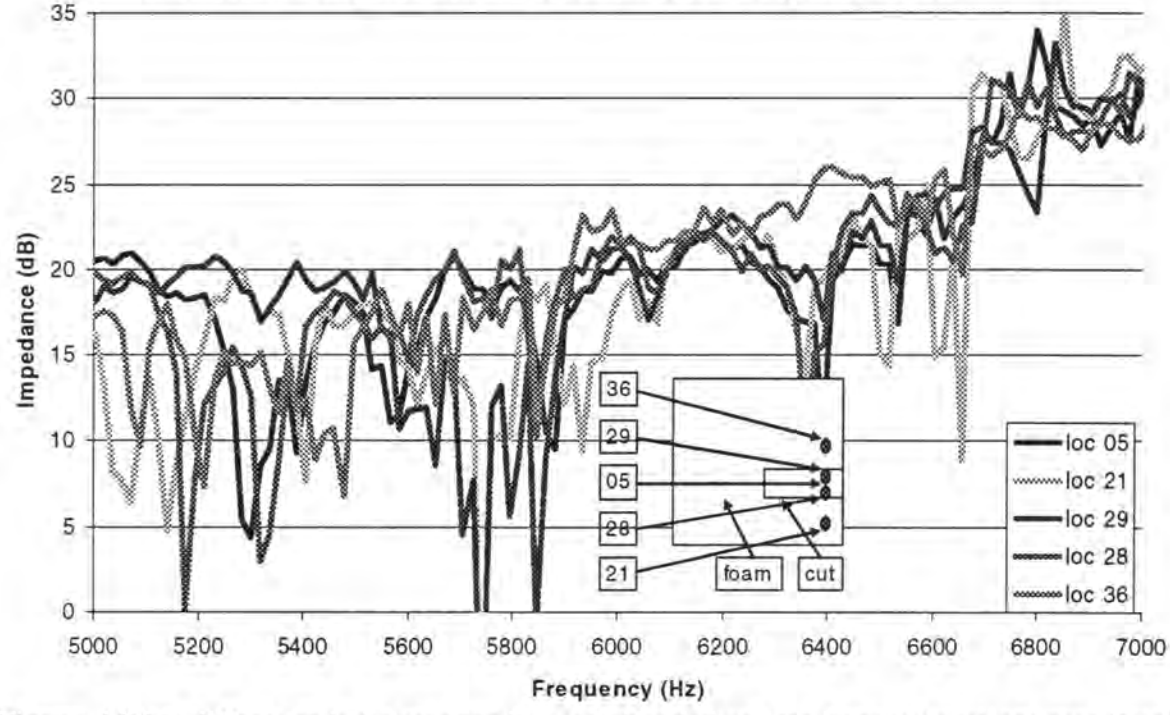

Figure 4.9 No difference in impedance between bonded and un-bonded locations was found on closer investigation of the 5000 to 7000 Hz frequency band.

The difference found at 2400 Hz was focused on as the most likely to produce an indicator of the bonding condition. When points 24 and 33 are examined, Figure 4.10, they continue to show a difference between these points over bonded locations and remaining points over the cut. Locations 24 and 33 are located 1.5 inches to the left and right of the cut respectively. In Figure 4.10 two new locations are compared to the locations already over the cut. These locations are 27 and 30 which occur directly over the edge of the cut. These locations do not show a difference between the locations over the cut and the locations over the edge of the cut. This indicates that the measurement of the impedance of the location over the edge of the cut is dominated by the impedance of the SOFI over the cut.

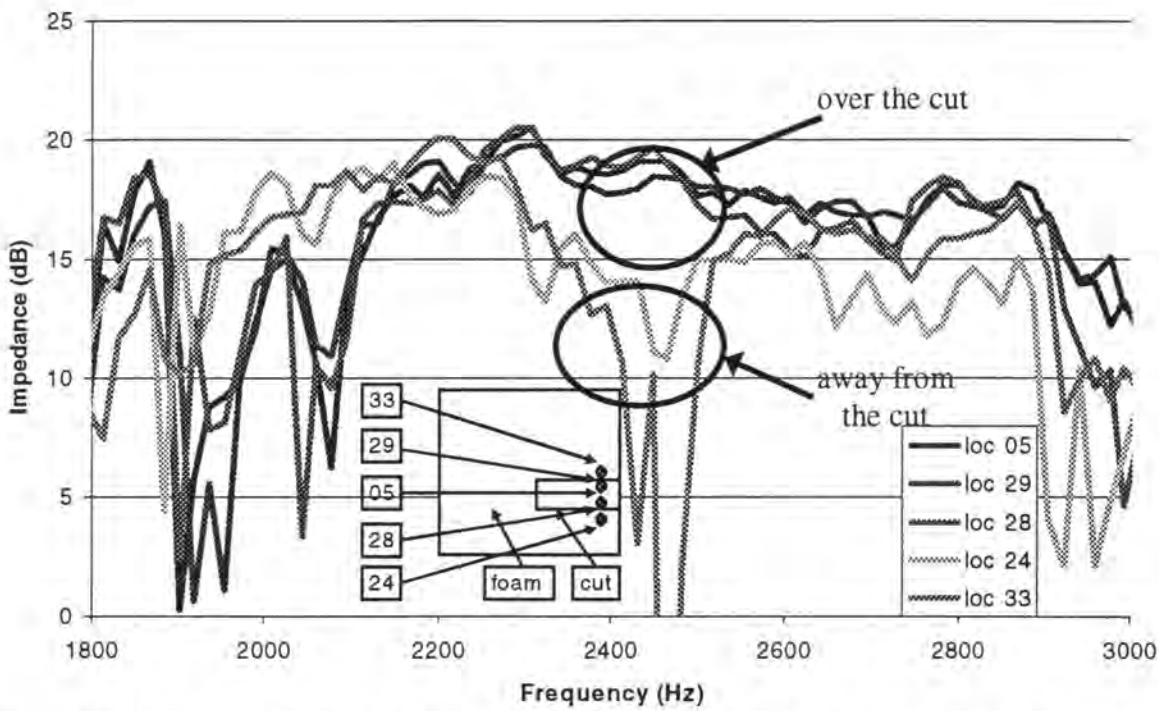

Figure 4.10 Difference in the real part of impedance visible for locations closer to the cut.

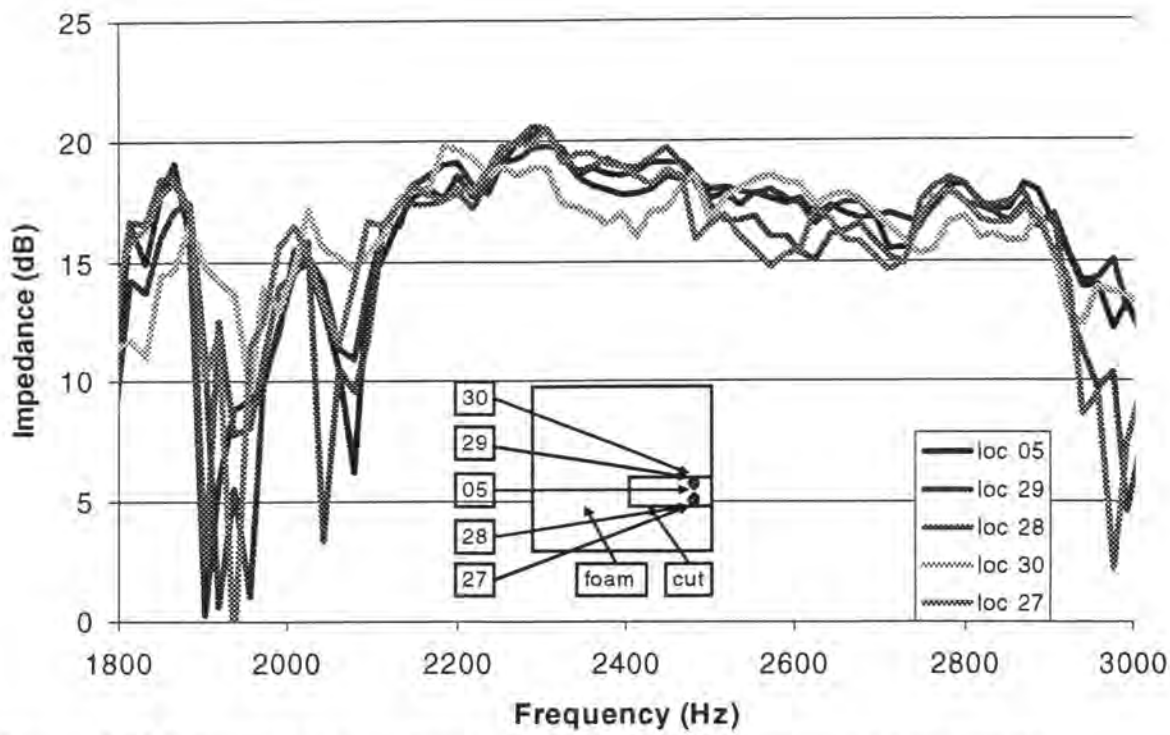

Figure 4.11 Difference in impedance disappears for measurements taken over the edge of the cut.

4.4 Indicators

Since frequency spectra for many locations are difficult to visually analyze, a single number is desired that will allow a decision to be made whether the point is over a bonded or un-bonded area. Two different methods for determining an indicator were attempted, Figure 4.12. First the real part of impedance was summed over a frequency range from 2360 to 2450 Hz, and second, the minimum value in the same frequency range was determined. The sum was done on the magnitude linear impedance scaled values and then the dB value was calculated while the minimum was the minimum of the dB scaled values, Figure 4.12.

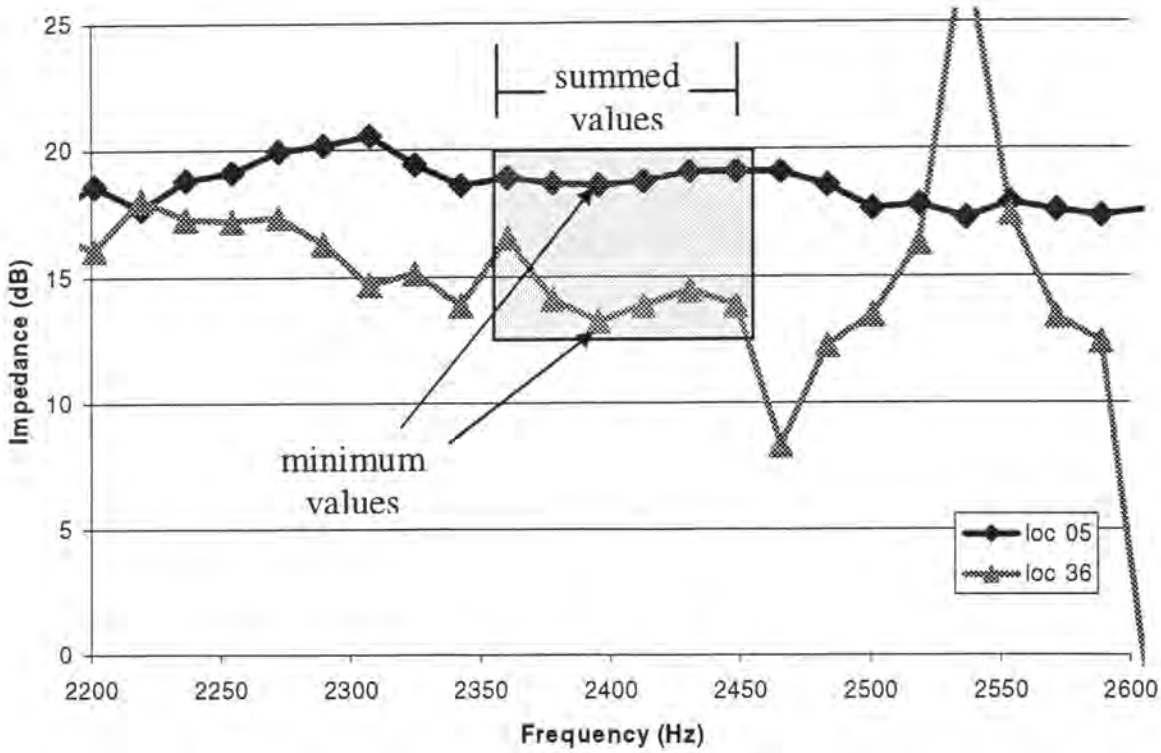

Figure 4.12 Points inside the gray box were summed or the minimum value of those points was found to create the indicators

The results from these two indicators are compared in Figure 4.13 for a line across the cut. The position of the cut is shown. Each indicator is 5 to 15 dB higher over the cut, compared to values over the bonded area. Further, only a 6 dB greater resolution is gained by using the minimum values rather than the sum. This increase is also only seen on a few points in the measurement. At most points the difference is less than one dB.

From the results summarized in Figure 4.13 it is possible to assume that the minimum indicator is preferred because of the slight advantage of the increased resolution, but Figures 4.14 and 4.15 from the measurements in the reverberant room, show that the minimum indicator is much more variable and does not produce as consistent an indication of the location of the cut as the sum indicator does. In the rest of this chapter only the sum indicator will be used. That the sum is the more reliable indicator shows that the effect of bonding on the impedance is more a frequency averaged effect than an effect at a single frequency.

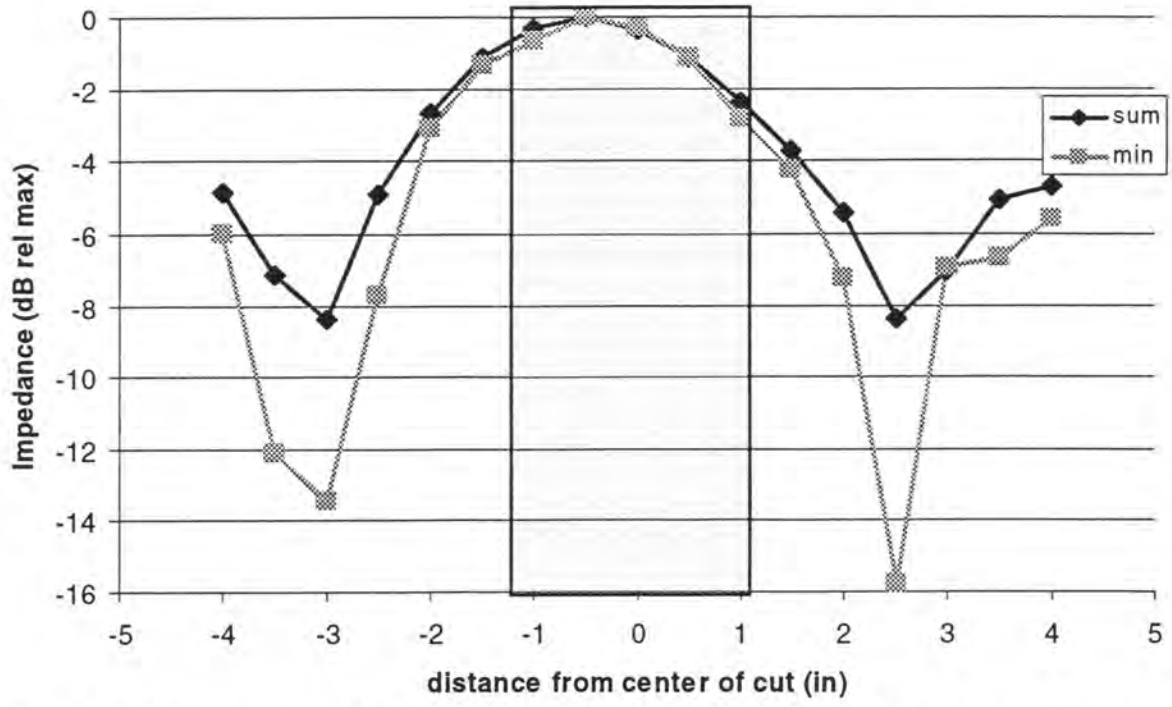

Figure 4.13 Comparing the min and sum indicators for a scan across the cut on measurements done in the anechoic chamber, the location of the cut is indicated by the gray box, 2400.Hz range.

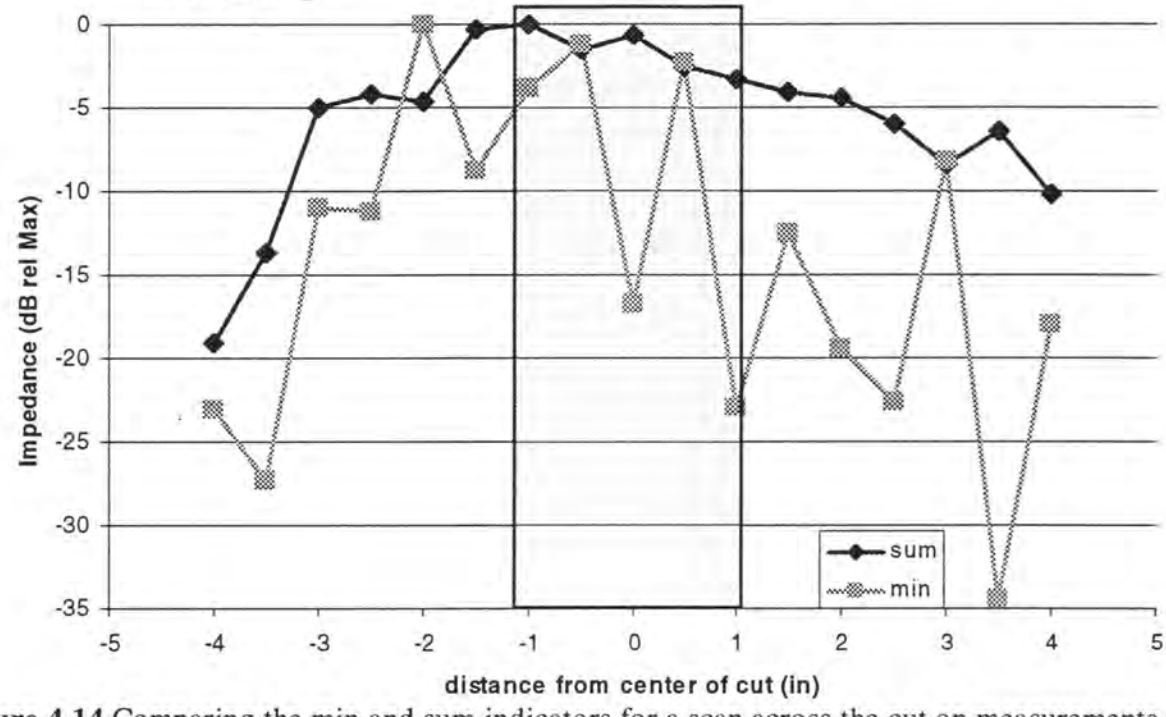

Figure 4.14 Comparing the min and sum indicators for a scan across the cut on measurements done in the reverberant room, the location of the cut is indicated by the gray box, 2600 Hz range.

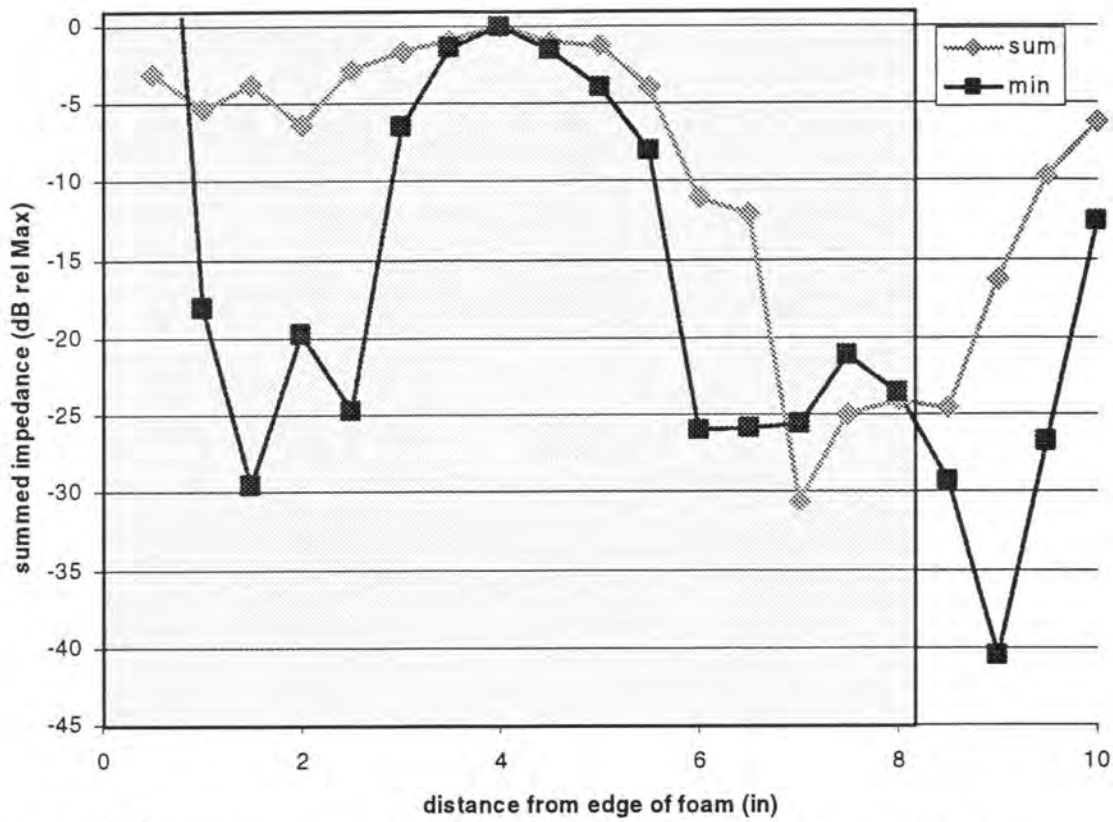

Figure 4.15 Comparing min and sum indicators for a scan along the cut, on measurements done in the reverberant room, the location of the cut is indicated by the gray box, 2600 Hz range.

4.5 Anechoic Chamber

Results from the anechoic chamber show good detection of the cut using the sum indicator, Figure 4.16. However, identification of the end of the cut in the scan along the length of the cut is inconclusive, Figure 4.17. The length of the cut is known to be 8 inches because of the known size of the piece of metal used to form the cut. Given that the grain of the SOFI is as shown in Figure 4.18a and as discussed in section 4.1, it is possible that the metal piece that was used to make the cut did not remain along the aluminum backing. If the cut were to deviate away from the back of the SOFI, the frequencies chosen for the indicator would be incorrect as the frequency that would show a difference would shift according to the depth of the cut from the surface of the SOFI sample. This is one possible explanation of the poor detection of the end of the cut.

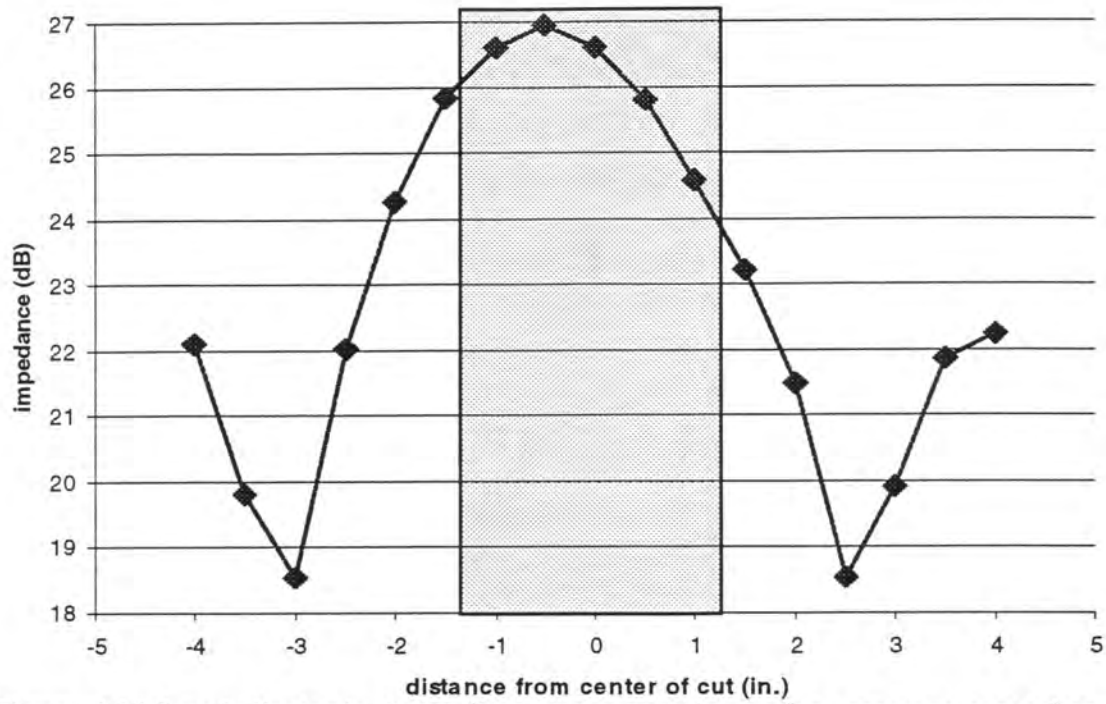

Figure 4.16 Sum indicator is shown for a scan across the cut for a measurement taken in the anechoic chamber, the location of the cut is indicated by the gray box, 2400 Hz range.

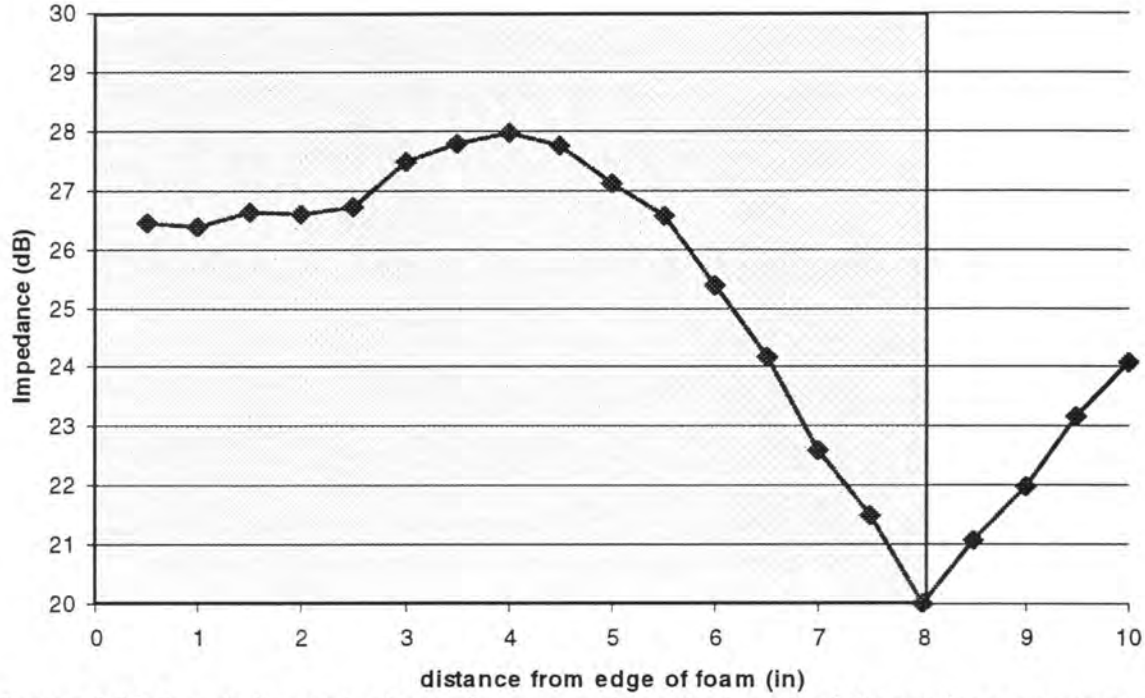

Figure 4.17 Sum indicator is shown for a scan along the length of the cut for a measurement taken in the anechoic chamber, the location of the cut is indicated by the gray box, 2400 Hz range.

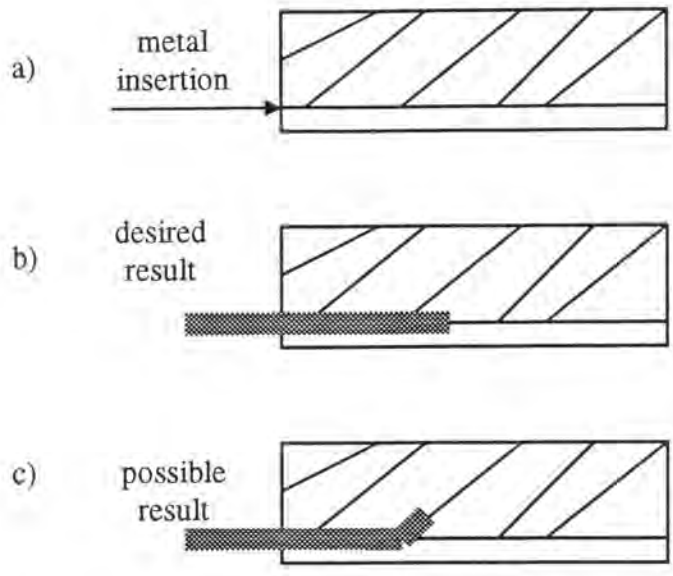

Figure 4.18 Possible explanation of poor detection of the end of the cut in scans along the cut, a) shows the direction of insertion for the metal piece, b) shows the desired un-bonded area to be created by the metal insertion, c)shows a result that could explain the poor detection of the end of the cut.

4.6 Reverberant Room

The reverberant room experiment was conducted carefully so that the only variable between this experiment and the experiment that took place inside the anechoic chamber would be the acoustic environment. The results show that the frequency difference noticed in the anechoic chamber in the 2400 Hz range is still present but the results are not as consistent as the results in the anechoic chamber. Instead the key frequency range in the reverberant room data for detecting bonding is around 2600 Hz, Figure 4.19.

This change in frequency may be a result of the anisotropic nature of the SOFI. When the SOFI sample was in the anechoic chamber tight control was maintained to eliminate any sound that would be reflected. Therefore the sound was incident from one direction. However, when the SOFI sample was placed in the reverberant room this control was lost and the sound from room reflections and ambient noise were incident from many directions. The sound that is not incident perpendicular to the SOFI surface, is effected by the angle of

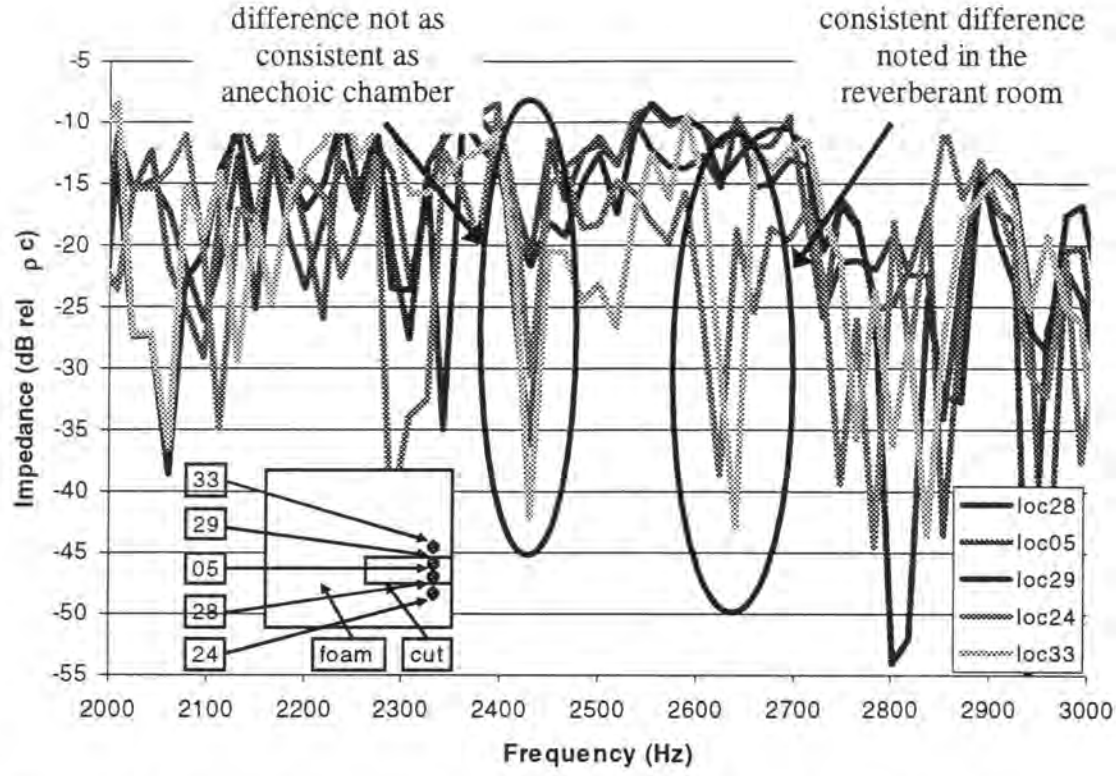

Figure 4.19 Change in frequency for difference in impedance between bonded and un-bonded areas from 2400 Hz in anechoic chamber to 2600 Hz in reverberant room.

incidence and the speed of sound in the SOFI material that may have depended on direction. Typically in characterizing the acoustic absorption or transmission loss of a material, there are different values for perpendicular or random incidence sound. Therefore the frequency shift seen in the reverberant room measurements is not altogether unexpected.

Processing of the reverberant room results used the data over a frequency range around 2600 Hz, 2624 to 2660 Hz. In Figure 4.20 it is again seen that the detection of the end of the cut in the scan along the length of the cut is not clear, while Figure 4.21 shows good detection of the cut, using the sum indicator at the 2600 Hz frequency in a scan across the cut.

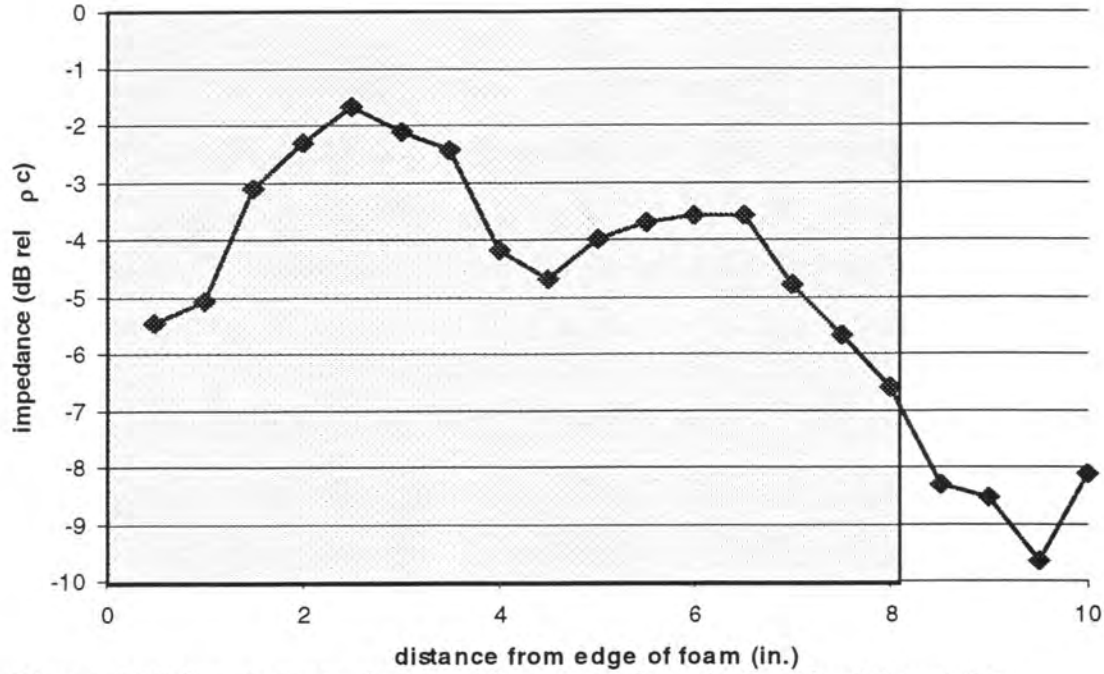

Figure 4.20 Sum indicator is shown for a scan along the length of the cut for a measurement taken in the reverberant room, the location of the cut is indicated by the gray box, 2600 Hz range.

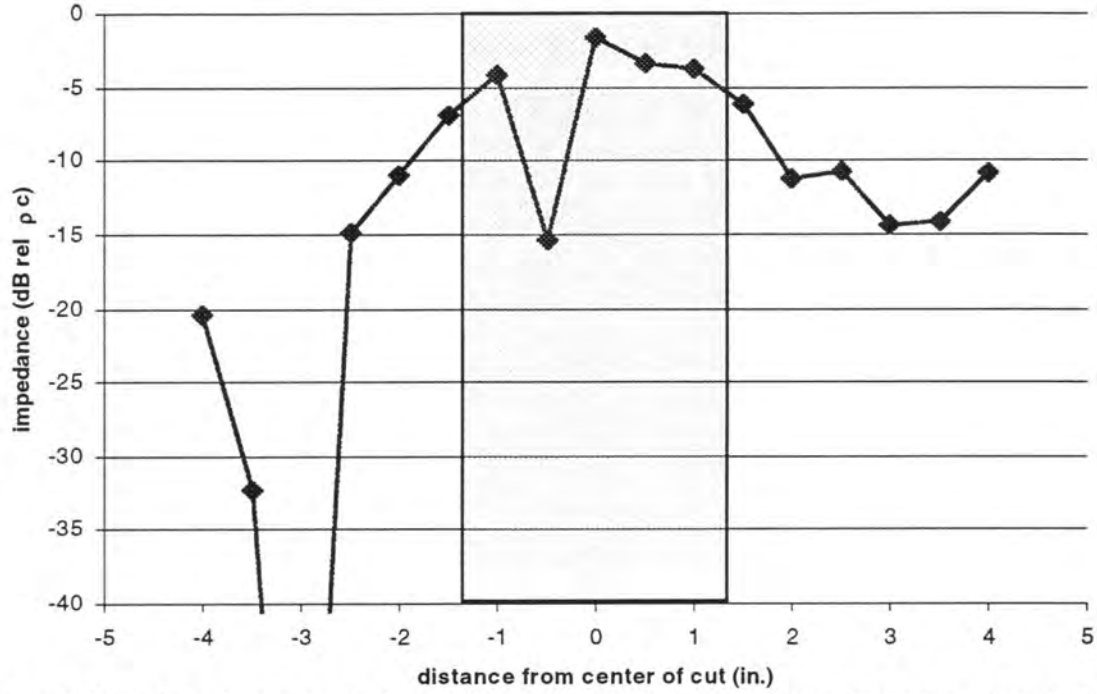

Figure 4.21 Sum indicator is shown for a scan across cut for measurements taken in the reverberant room, the location of the cut is indicated by the gray box, 2600 Hz range.

4.7 Moving Source

In the moving source measurements, the source was moved to always be directly above the microphones. The goal of this experiment was to keep the relationship between the source and the microphone and holder combination the same. This was to have eliminated any dependence of the result on changing the relationship between the source and the microphones.

As can be seen in the Figures 4.22 and 4.23, the moving source does not produce as consistent results as the stationary source, Figures 4.20 and 4.21. It is much more difficult to identify where the cut is when the source is moving. From the results in Figures 4.22 and 4.23 it is seen that the moving source actually degrades the ability of the sum indicator of bonding to detect the cut.

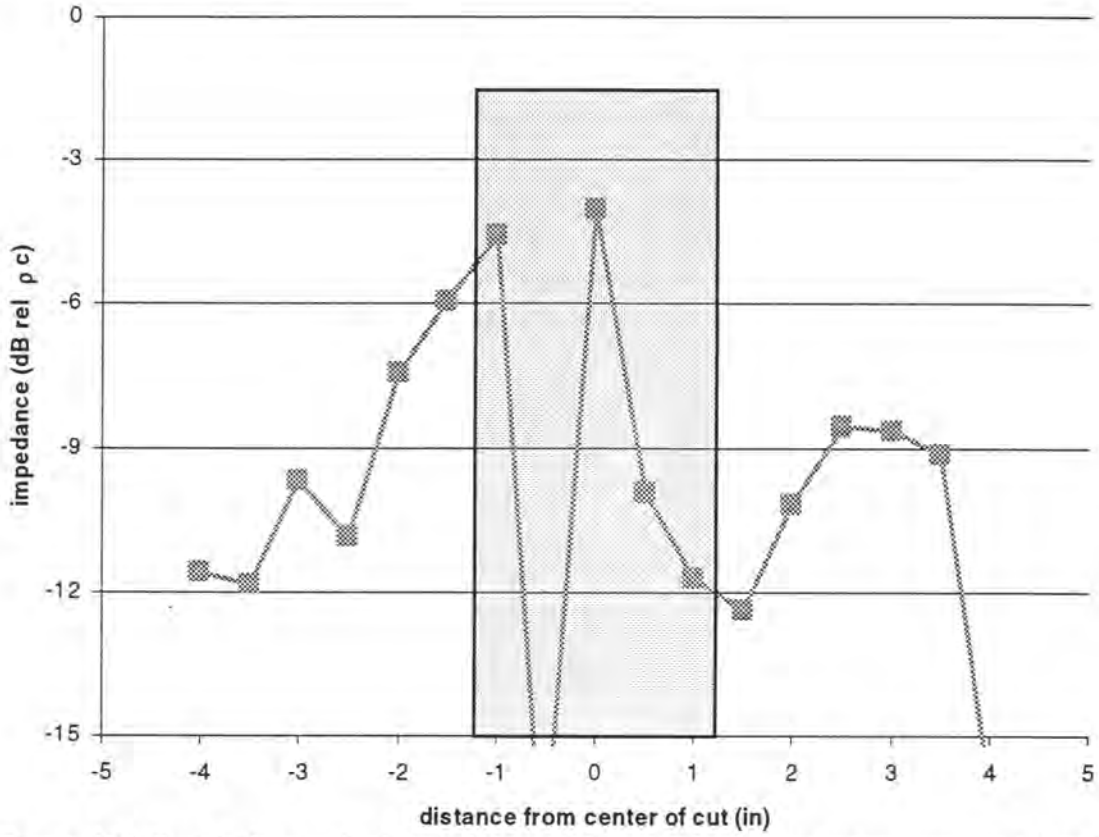

Figure 4.22 Sum indicator is shown for a scan across the cut for measurements taken in the reverberant room, with a moving source, 2600 Hz range.

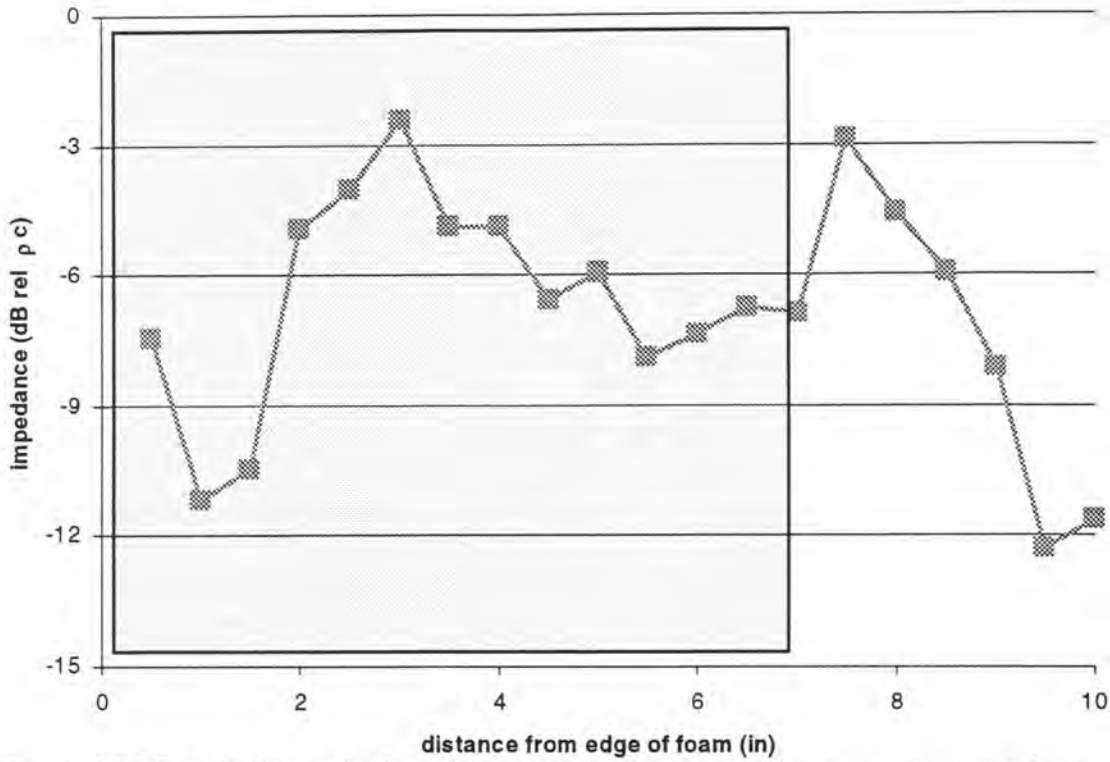

Figure 4.23 Sum indicator is shown for a scan along the cut for measurements taken in the reverberant room, with a moving source, 2600 Hz range.

4.8 Impedance tube

The impedance tube experiment had the goal of providing a more robust measure of impedance that would be portable and easy to implement in a real situation. The impedance tube takes care of two problems inherent in the free-field measurements. First, in the free-field measurements it is simply assumed that the acoustic field is planar at the SOFI surface. With the impedance tube it is guaranteed that the acoustic field is planar up to the frequency that has a wavelength that is twice the size of the tube diameter. Second, the free-field measurements are susceptible to outside noise and the reflections from nearby surfaces. The impedance tube should isolate the acoustic field in the tube from outside noise, this includes both ambient noise and undesired reflections of the noise used to make the impedance measurement.

Three different tube lengths were chosen, 15 inches, 16.5 inches and 18 inches. This decision was made to avoid possible problems with resonance in the length of the tubes. The

concern was that the tube length could change the impedance at the end of the tube at a frequency where the tube length corresponds to a multiple of the wavelength.

Figure 4.24 shows the result for the impedance measurement in the 15 inch tube over the center of the cut. This result is interesting when compared with Figure 4.1. The results from the impedance tube are much more smooth with less variation over small frequency ranges.

Figures 4.24 through 4.27 show the real part of impedance at the measurement plane for the three tube lengths. This was the part of the impedance measurement that was focused on in earlier measurements, so it is continued to be investigated here. The three tube lengths show almost identical impedance measurements. Also, more importantly, there is no indicator that shows which locations are bonded or un-bonded.

Figure 4.28 shows that the impedance measured does not vary for the various tube lengths. The reason the impedance does not vary for tube length or location may be that the equations applied to the free field measurement do not work in the impedance tube. The data taken with the impedance tube was analyzed using the same program as the free field data. If methods designed for use in impedance tubes were used the data may show some differences.

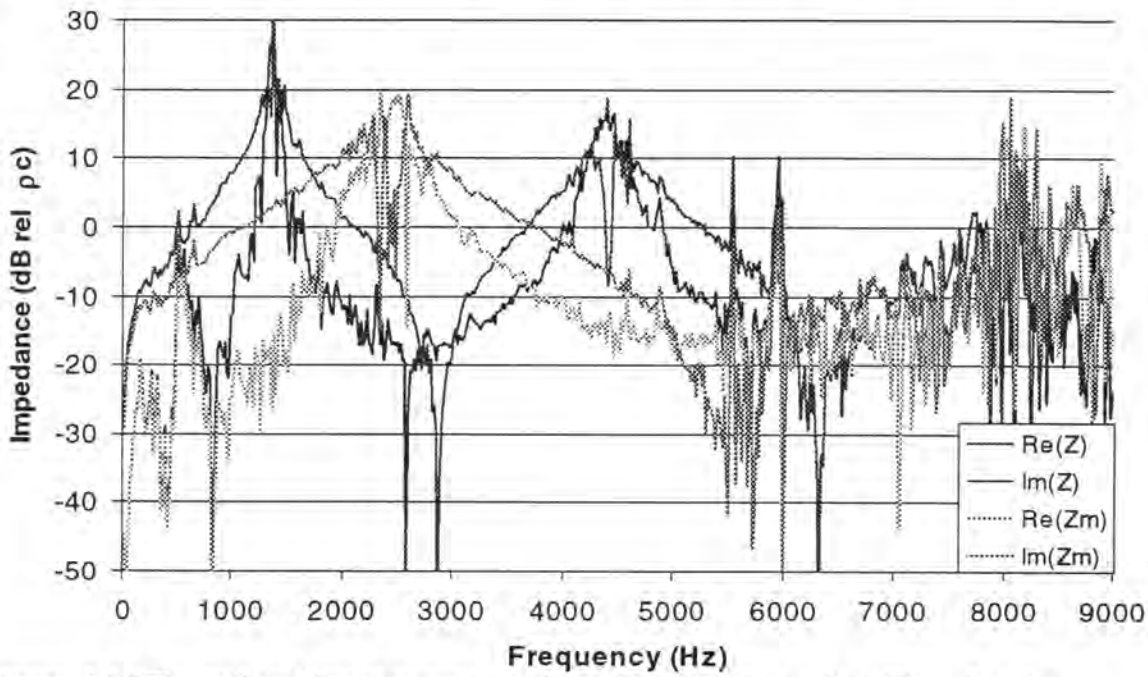

Figure 4.24 The real and imaginary parts of impedance at the surface (Z) and at the measurement plane (Zm) for a measurement over the center of the cut with the 15 inch tube.

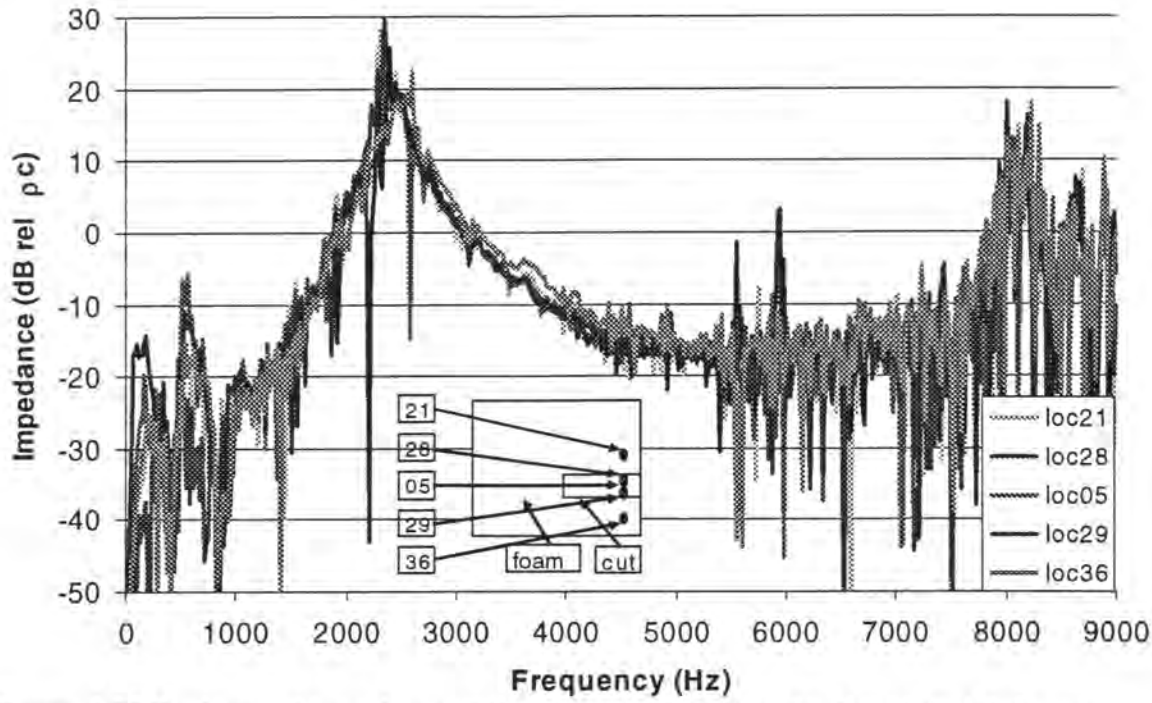

Figure 4.25 Real part of impedance at the measurement plane for the 15 inch tube, no differences are visible between the bonded and un-bonded locations

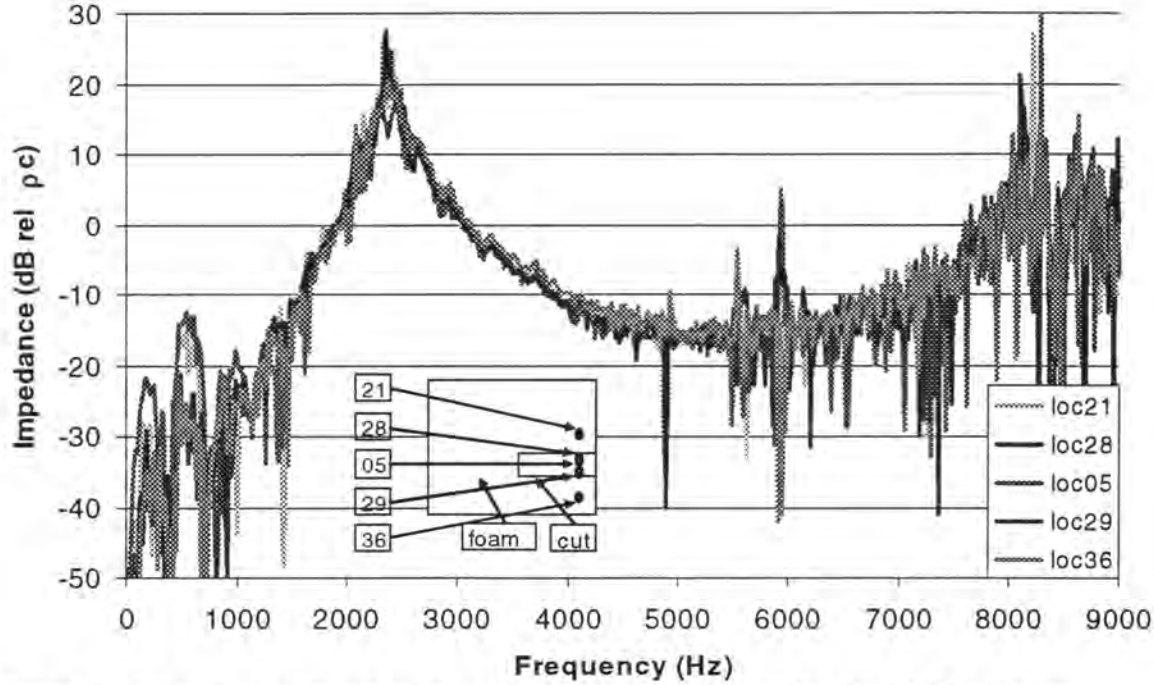

Figure 4.26 Real part of impedance at the measurement plane for the 16.5 inch tube, no differences visible between the bonded and un-bonded locations

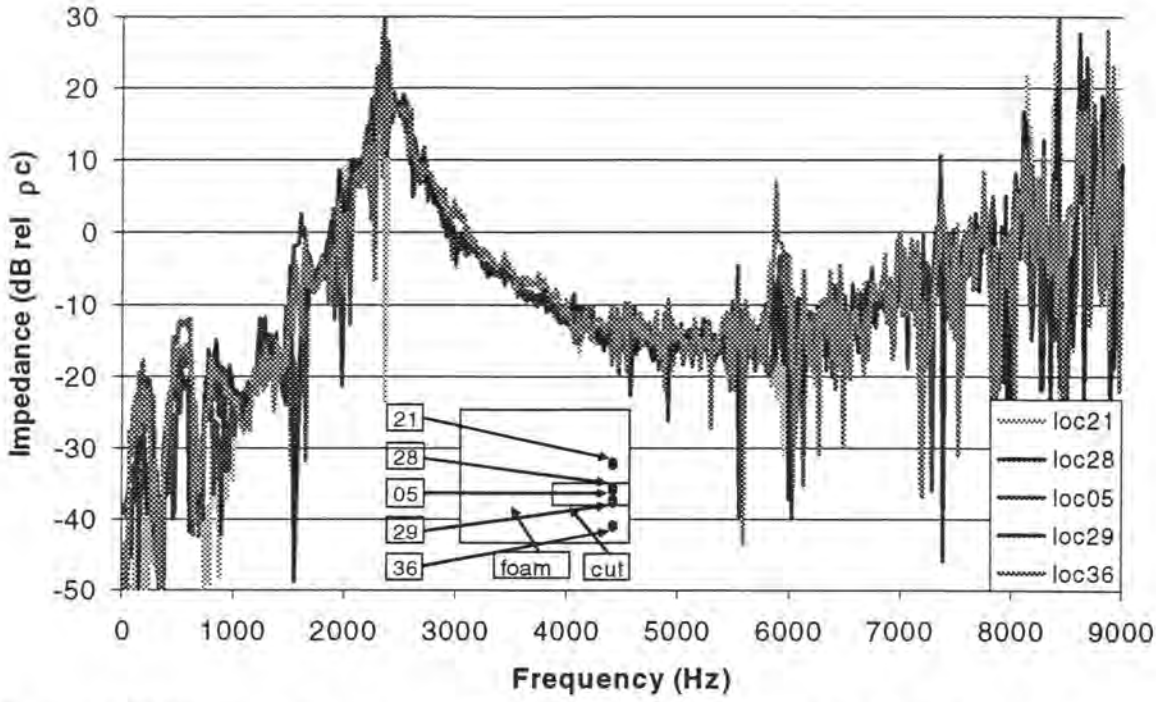

Figure 4.27 Real part of impedance at the measurement plane for the 18 inch tube, no differences visible between the bonded and un-bonded locations

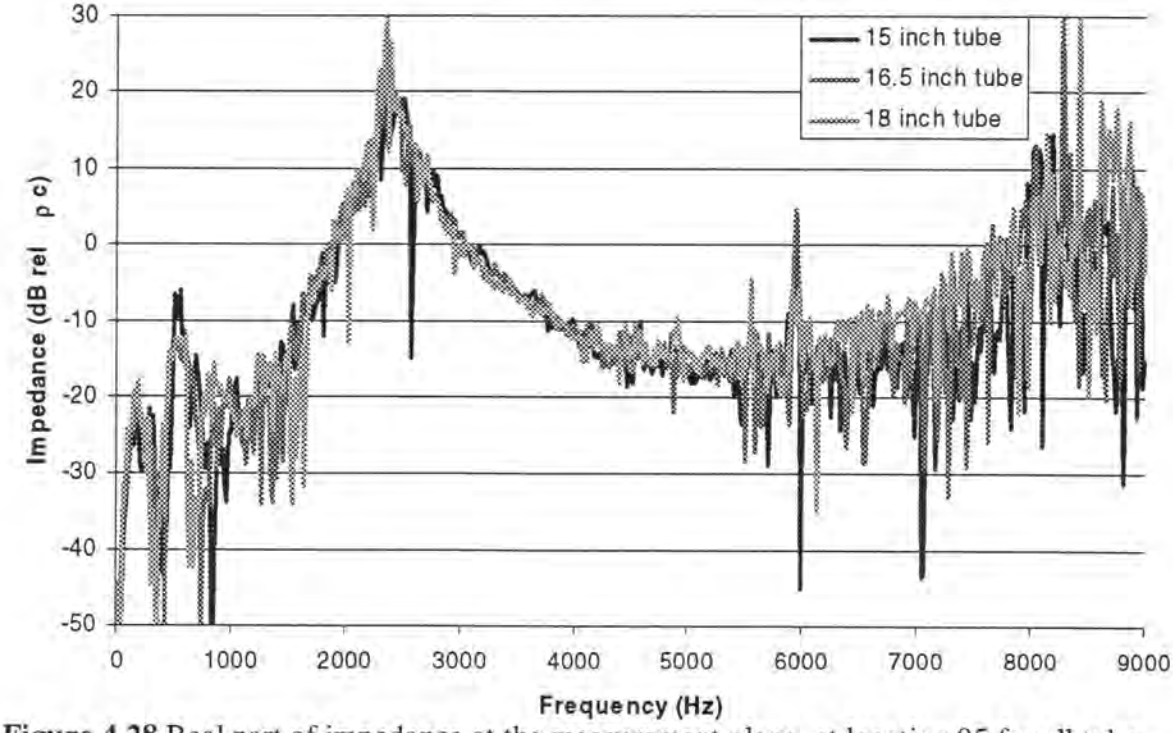

Figure 4.28 Real part of impedance at the measurement plane, at location 05 for all tube lengths, no difference is seen based on tube length.

4.9 Comparing Conditions

Figure 4.28 shows the sum indicator for a line of measurements taken along the cut in each of the first three experiments. Figure 4.29 shows the sum indicator for a line of measurements taken across the cut in each of the first three experiments. The data from the experiment in the anechoic chamber were calculated around 2400 Hz and the data for both experiments in the reverberant room were calculated around 2600 Hz. The measurement in the anechoic chamber has the most consistent trend, and the one that identifies the cut the most clearly. The measurement in the reverberant room also shows good detection of the cut. This is important because in a real implementation this measurement is unlikely to be done in an anechoic chamber. The measurements taken with the moving source do not give a clear indication of the location of the cut. This indicates that retaining the relationship between the source and the microphones actually degrades the quality of the measurement.

These graphs also give an indication of the spatial resolution of the measurement. For most of the locations the next measurement is within 1 dB. This means that the spatial resolution of the measurement is around 1 inch, i.e. measurements must be 1 inch apart in order to be differentiable. It would be expected that a measurement of the same point would vary on the order of 1 dB if the measurement were repeated. A 1 inch resolution also supports the assumption of locally reacting because 1 inch is much less than a wavelength for frequencies near 2500 Hz. This resolution should be tested to determine the size of defects that can be detected by this method.

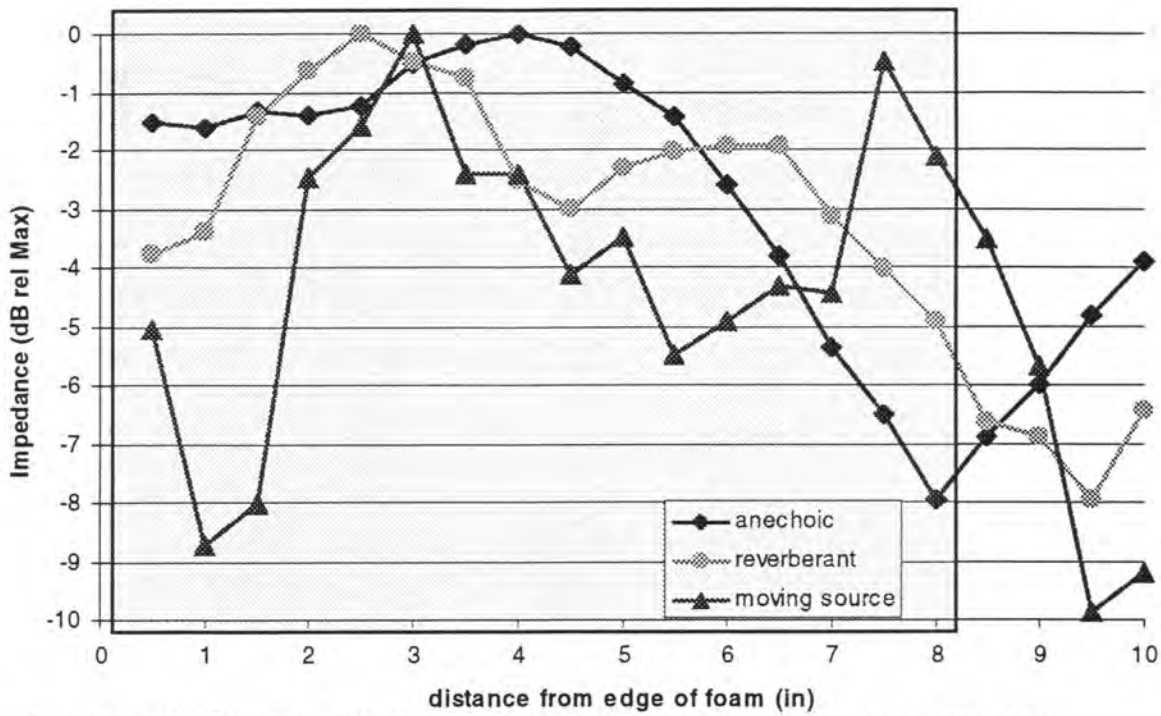

Figure 4.29 The sum indicator for measurements along the cut for the anechoic chamber experiment, the reverberant room experiment and the moving source experiment.

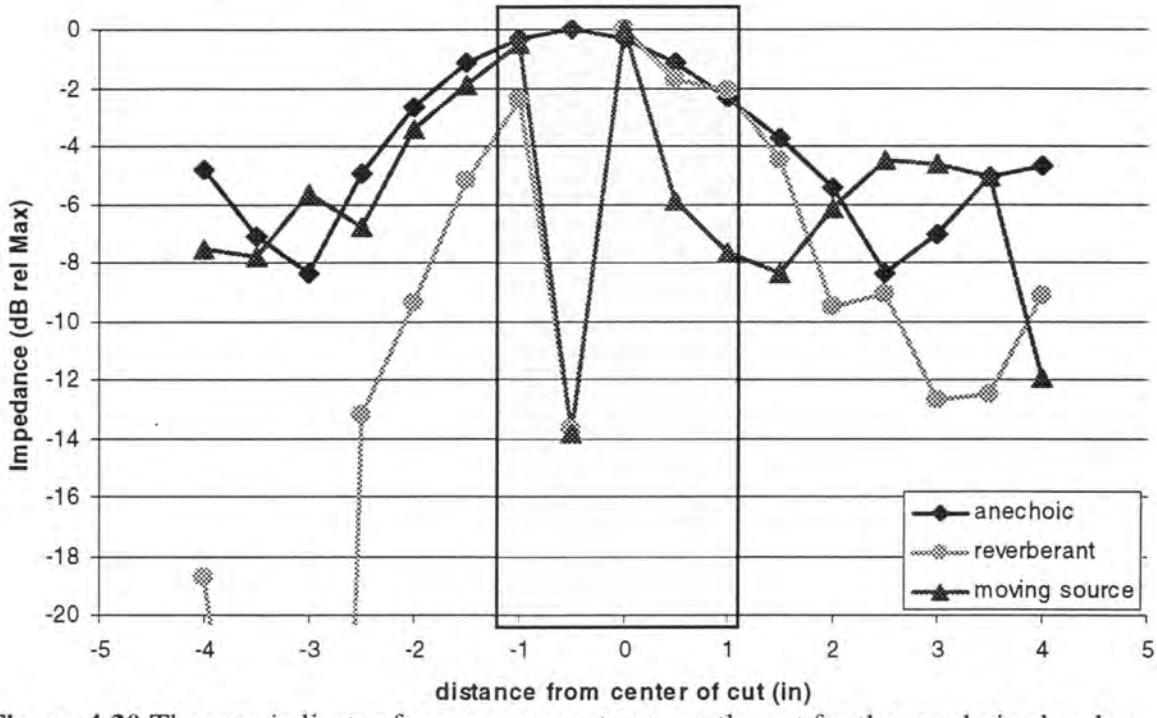

Figure 4.30 The sum indicator for measurements across the cut for the anechoic chamber experiment, the reverberant room experiment and the moving source experiment.

CHAPTER 5. SUMMARY AND CONCLUSION

This section will summarize the work done, explain the conclusions and suggest items for future work.

5.1 Summary

Four experiments were done on the NASA SOFI sample. One was done in the anechoic chamber and three were done outside the anechoic chamber. The measurements in the anechoic chamber were done first because the environment eliminated reflected and background sound that would make results more difficult to analyze. Of the measurements outside the chamber the first experiment was done to see if the measurement was possible in a reverberant environment. The second experiment outside the chamber was done to see if moving the source along with the microphones would produce a better measurement. The final experiment was done to see if an impedance tube could be used to measure the impedance of the SOFI sample.

5.2 Conclusions

It is possible to measure the impedance of the SOFI surface, and the impedance of the SOFI surface does indicate the bonding condition. Measurements in the anechoic chamber produced clear indicators of the bonding condition. Measurements in the reverberant room produced good indicators of the bonding condition, but were not as clear as the indicators in the anechoic chamber. Measurements with a moving source did not produce good results, indicating that keeping the same relationship between the source and the microphones is not advantageous to the identification of the bonding condition.

Two indicators of the impedance change were developed, the sum and the minimum. Both the sum and minimum indicators worked well in the anechoic chamber with the minimum indicator providing slightly higher resolution. However, the sum worked much better in measurements taken outside the chamber. The frequency chosen to represent the change in bonding condition inside the anechoic chamber was near 2400 Hz. This is somewhat expected because the theory shows that the impedance of the surface should be more sensitive to the impedance of the SOFI-aluminum interface at a resonant frequency, around 2500 Hz for the thickness and assumed speed of sound in the SOFI sample. When the sample was measured in the reverberant room, the frequency chosen to represent the bonding condition was near 2600 Hz. The reason for this shift in frequency may be that the reflections present in the reverberant room caused the impedance measurement to be more sensitive to the anisotropic nature of the SOFI.

The spatial resolution observed in the measurements is around 1 inch. This is much less than a wavelength for the frequencies that were of interest. This supports the assumption that the SOFI is locally reacting.

The impedance tube produced results that were identical across all locations. This indicates that the impedance being measured was that of some part of the impedance tube and not that of the SOFI. The impedance tube did not work as expected but is a very desirable measurement to make because it guarantees plane waves and isolates the measurement from the environment. Because of the desirable qualities of the impedance tube measurement, more work should be done on that type of measurement to produce one that works well.

5.3 Future Work

While it has been shown that acoustic impedance can be used as an indicator of the bonding condition of SOFI to its aluminum backing, more work needs to be done in this area.

The impedance tube was unable to produce good results. The impedance tube measurement has the advantages of being isolated from the environment, and guaranteeing the plane waves required for the impedance measurement up to a frequency where the ½

wavelength is equal to the diameter of the tube. The measurement using the impedance tube also has the advantage of provide a small, known area that is being measured. This makes the impedance tube a good method to use for practical implementation. More work should be done to develop the impedance tube method.

Another useful measurement would be the implementation of a scanning system, so the whole sample could be analyzed. An automated scanning system would allow data to be taken over the entire sample. This was not possible doing the measurements by hand because of the time required to move the microphones and then acquire the data. The decision was made to simply take a few points that are likely to show differences. The acquisition of data at a point takes approximately 10 seconds. The moving of the microphone means that a measurement can only be taken once per minute. The data provided by a 2-D scan of the entire surface of the SOFI sample would be useful. It could also be used to better define the spatial resolution of the measurement and determine the minimum size of cuts that can be detected by this method. For example, it is possible that it will be easier to detect the edge of the un-bonded area rather than the un-bonded area itself. Large dips in the sum indicator were noticed just outside the un-bonded areas, if this behavior is typical of edges between bonded and un-bonded areas, it would be simple to identify the edge of an un-bonded area. This is not currently known because data has only been examined for 3 places where a line of measurements crosses an edge, and one of those places, the line down the center of the SOFI sample, the behavior of the cut is uncertain at the end.

It would also be desirable to know the geometry of the cut. In order to know the geometry of the cut, the sample would have to be dissected. This would allow a determination if the cut deviated from the aluminum backing as is suspected from the measurements and the nature of the SOFI sample grain.

The deviation of the cut from the aluminum backing creates another situation that NASA is concerned with. That of an air gap located somewhere in the SOFI material but not at the SOFI-aluminum interface. If the depth of the air gap is known, this should be a simple extension of the work that has been done already.

There were some initial measurements that appeared to indicate that impedance at higher frequencies may depend on the relationship between the microphone holder and the

speaker. These frequencies may be important because they range from ½ to ¾ wavelengths. It has already been shown that the ¼ wavelength frequency shows the bonding condition; these frequencies may also show the bonding condition or show the bonding condition better than at the ¼ wavelength frequency that was chosen as the indicator of the bonding condition. More work should be done to determine the influence of the microphone holder position on the impedance measurements.

Impedance measurements can also be applied to other situations where it is desirable to know the bonding condition or see through a surface. One possible application of this would be to determine the effectiveness of the insulation in a refrigerator wall. Currently a heat source is used inside the refrigerator and thermal images are taken outside to determine if the insulation is present in all areas of the refrigerator walls. This measurement was done for a similar situation, insulating foam with a metal backing. It may be possible to use the impedance measurement to determine the presence of foam insulation inside the metal refrigerator shell, if the presence or absence of foam insulation is assumed to change the impedance of the foam-shell interface. It may not even be necessary to use a noise source for the measurement if the test is done on the factory floor, which typically has fairly high noise levels. The noise would also typically be diffuse, originating from all directions, which may or may not be desirable. This would have to be investigated as the requirement for the impedance measurement is that the acoustic field is planar.

This measurement could be used to detect anything that would be expected to change impedance of the surface of a material, whether the change in impedance occurs in the material itself, or in a substrate that would affect the impedance of the surface. This measurement may be able to be used to measure the density of plywood or MDF, the bonding of metal sheeting to core plywood in a wooden core storm door, the presence of insulation in the walls of a house, the structural condition of the walls of a house, or even the liquid level in a tank.

The acoustic impedance measurement performs well as an indicator of the bonding condition of SOFI to a metal backing. There are other applications for which the same measurement may be successful, applications where the change to be identified can be reasonably assumed to change the acoustic impedance at some point in the material. More

work should be done to refine the impedance measurement on the SOFI, and to expand the impedance measurement to other applications.

REFERENCES

Abraham, D., C. Carles, and J. C. Pascal. 2nd International Congress on Acoustic Intensity. Mesure in-situ de l'impedance acoustique des materiaux en fonction de l'angle d'incidence. Senlis, 1985.

Allard, J. F., and A. Akine. "Acoustic Impedance Measurements with a Sound Intensity Meter." Applied Acoustics. 18 (1985) 69-75.

Allard, J. F., R. Bourdier, and A. M. Bruneau. "The Measurement of Acoustic Impedance at Oblique Incidence with Two Microphones." J. Sound Vib. 101 (1985): 130-132.

Allard, J. F., and P Delage. "Free Field Measurements of Absorption Coefficients on Square Panels of Absorbing Materials." J. Sound Vib. 101 (1985): 161-170.

Allard, Jean-Francis, Walter Lauriks, and Christine Verhaegen. "The acoustic sound field above a porous layer and the estimation of the acoustic surface impedance from free-field measurements." J. Acoust. Soc. Am. 91 (1992): 3057-3060.

Allard, Jean F., and Benita Sieben. "Measurements of Acoustic Impedance in a Free Field with Two Microphones and a Spectrum Analyzer." J. Acoust. Soc. Am. 77 (1985): 1617-1618.

Blaser, D. A., and J. Y. Chung. "Transfer function method of measuring in-duct acoustic properties. I. Theory." J. Acoust. Soc. Am. 68 (1980): 907-913.

Bruneau, Anne-Marie, and Jean-Pierre Dalmont. "Acoustic Impedance measurement: Plane-wave mode and first helical mode contributions." J. Acoust. Soc. Am. 91 (1992): 3026-3033.

Chandler-Wilde, S. N., and K. V. Horoshenkov. "Pade approximants for the acoustical characteristics of rigid frame porous media." J. Acoust. Soc. Am. 98 (1995): 1119-1129.

Columbia Accident Investigation Board. Report Volume 1. Washington D. C., 2003.

Cops, A., and W. Lauriks. 2nd International Congress on Acoustic Intensity. Application of new two-microphone techniques to measure sound absorption characteristics of acoustic materials. Senlis, 1985.

Cramond, A. J., and C. G. Don. "Reflection of impulses as a method of determining acoustic impedance." J. Acoust. Soc. Am. 75 (1984): 382-389.

Dickinson, P J., and P E. Doak. "Measurement of the Normal Acoustic Impedance of Ground Surfaces." J. Sound Vib. 13 (1970): 309-322.

Don, C. G., and D. E. P. Lawrence. "Impulse measurements of impedance and propagation constant compared to rigid-frame and dual-wave predictions for foam." J. Acoust. Soc. Am. 97 (1995): 1477-1485.

Elko, G. E. "Frequency Domain Estimation of the Complex Acoustic Intensity and Energy Density." Ph.D. Thesis, The Pennsylvania State University 1984.

Fahy, F. J. Sound Intensity. London: Elsevier Applied Science, 1989.

Hollin, K A., and M H. Jones. "The Measurement of Sound Absorption Coefficient in Situ by a Correlation Technique." Acustica. 37 (1977): 103-110.

Irie, Yoshihiko, Tadao Nakamura, and Shigeru Takagi. 2nd International Congress on Acoustic Intensity. Application of acoustic intensity method to absorption coefficient measurement. Senlis, 1985.

Lahti, Tapio. 2nd International Congress on Acoustic Intensity. Application of the intensity technique to the measurement of impedance, absorption and transmition. Senlis, 1985.

Legouis, T., and J. Nicolas. 2nd International Congress on Acoustic Intensity. Determination of the specific normal impedance of a materiau by the phase gradient. Senlis, 1985.

Lord, Harold W., William S. Gatley, and Harold A. Evensen Noise Control for Engineers. Malabar, Florida: Robert E Krieger Publishing Co., Inc., 1987.

Mann, J. A. "Acoustic Intensity: Energy Transfer, Wave Properties and Applications" Ph.D. Thesis, Pennsylvania State University 1988.

Ross, D. F., and A. F. Seybert. "Experimental determination of acoustic properties using a two-microphone radom-excitation technique." J. Acoust. Soc. Am. 61 (1977): 1362-1370.

"Terahertz Technique for Shuttle Defects." Ed. Gopal Narayanan. NDT Update 12 (2003): 1-2.